Comparing 3D Point Clouds from Image-based Matching Method and Airborne LiDAR in Tropical Rainforest Reserve of Ayer Hitam, Malaysia.

PHANINTRA SOONTHORNHARUETHAI
May, 2016

SUPERVISORS:
Drs. E.H. Kloosterman
Dr. Y.A. Hussin

Comparing 3D Point Clouds from Image-based Matching Method and Airborne LiDAR in Tropical Rainforest Reserve of Ayer Hitam, Malaysia.

PHANINTRA SOONTHORNHARUETHAI
Enschede, the Netherlands, May, 2016

Thesis submitted to the Faculty of Geo-Information Science and Earth Observation of the University of Twente in partial fulfilment of the requirements for the degree of Master of Science in Geo-information Science and Earth Observation.
Specialization: Geo-information Science and Earth Observation for Environmental Modelling and Management (GEM)

SUPERVISORS:
Drs. E.H. Kloosterman
Dr. Y.A. Hussin

THESIS ASSESSMENT BOARD:
Prof.Dr. A.D. Nelson (Chair)
Dr. Tuomo Kauranne (External Examiner, Lappeenrantan University of Technology, Finland)

ABSTRACT

The study aimed to compare the quality of 3D point clouds from image matching method and airborne LiDAR in tropical rainforest reserve of Ayer Hitam, Malaysia for potential carbon study. Trees height, trees crown surface and crown height are used as the inventory variables to compare in individual tree based approach. The distance between point clouds is measured by point-to-point method. The method contains three parts: data pre-processing, data processing and data analysis. The first part related to the back-engineering to solve the problem of missing coordinates, bundle block adjustment and point clouds generation from aerial photographs. Secondly, the data processing stage is about the registration of point clouds and segmentation. The last part contained the whole data analysis of all inventory variables.

The result shows that there is no significance difference between point clouds from LiDAR and image matching method on tree height, tree crown surface and crown height. It is found during comparison that crown height which the image-based point clouds is differed from LiDAR point clouds by around 11 percent, while the NMSE is 17.2 % and R^2 is 0.91.
While the tree height and tree crown surface from image-based point clouds differed from LiDAR point clouds, which are around 25% and 29% respectively. The coefficient of determination (R^2) are 0.54 and 0.79 while the NRMSE (Normalized Root Mean Square Error) are 48% and 55% respectively

This study shows that the image-based point clouds can replace the usage of LiDAR point clouds for the assessment of crown height. Moreover, in the situation that, where ground point information like solitary trees or standalone trees can be extracted from aerial photographs, the image-based point clouds can replace LiDAR based point clouds.

Keywords: Airborne LiDAR, stereophotogrammetry, image-based point clouds, image matching, biomass, MRV, REDD+

ACKNOWLEDGEMENTS

This 22 months have been an intensive period of my life. I gained a lot of experience and knowledge during this time. I would like to reflect on the people who have supported and helped me throughout this period.

First of all, I would like to thank you my first cool supervisor, Drs. E.H. Kloosterman, for being as my Dutch father and have been taking care of me all the time in Enschede and also during the fieldwork in Malaysia. Thank you for being such a great supervisor, encourage person and always there whenever I need any helps not only for the study but also life suggestion and motivation. I would like to thank you Dr. Y.A. Hussin, for the excellent supervised and suggested this amazing research topic to me. Thank you for always be kind to me and guide me to the right path of the study.

Special thanks to University Putra Malaysia and all the forest rangers in Ayer Hitam Forest Reserve for all the hard works together and very nice suggestions.

I would particularly like to thank my fellow student in GEM course for their wonderful collaboration. To Laura, Emile, Noshan and Mirza. Thank you for your valuable guidance for being together like a family and sharing perfect experiences for the study and for life.
They have been and always be there to support me. Thanks to all NRM and ITC friends for always be nice, caring and supportive.

I would also like to express my gratitude to Royal Thai Air Force for giving me the opportunity to study in this master program. Thank you FMV (Försvarets Materielver) especially Col. Per Lennerman who always be supportive and gave an excellent cooperation during this wonderful two years.

Lastly, I would like to thank my parents for all supported and sympathy. Thanks to all friends and all my beloved who always listen, encourage and being nice consultants in everything.

Phanintra Soonthornharuethai
Nakhonpathom, Thailand
May, 2016

TABLE OF CONTENTS

LIST OF FIGURES

LIST OF TABLES

LIST OF ABBREVIATION

AGB	Above Ground Biomass
AHFR	Ayer Hitam Forest Reserve
ALS	Airborne Laser Scanner
BGB	Below Ground Biomass
DBH	Diameter at Breast Height
DSM	Digital Surface Model
DTM	Digital Terrain Model
ICP	Iterative Closest Point
IMB	Image - based matching
IPCC	Intergovernmental Panel on Climate Change
LiDAR	Light Detection And Ranging
MTPs	Manual Tie Points
NRMSE	Normalized Root Mean Square Error
REDD+	Reducing Emissions from Deforestation and Forest Degradation
RMSE	Root Mean Square Error
RTAF	Royal Thai Air Force
TLS	Terrestrial Laser Scanner
UAV	Unmanned Air Vehicle
UNFCCC	United Nation Framework Convention on Climate Change
UPM	University Putra Malaysia

1. INTRODUCTION

1.1. Background

According to the fifth assessment report by IPCC(2014), the anthropogenic greenhouse gases (GHG), namely carbon dioxide (CO_2), methane (CH_4) and nitrous oxide (N_20) have been increasingly emitted since 1970, with larger absolute increases between 2000 and 2010. Besides, CO_2 is the most emitted gas compare to other GHG and generally released from forestry, land use, fossil fuel, cement production and flaring. These GHG, especially CO_2, are trapping the thermal energy reflected back from Earth to the atmosphere and consequently creating "global warming" phenomenon. Undoubtedly, it also affects the change of climate around the world.

Forests are the storehouses of carbon and absorbent sources of carbon dioxide from the atmosphere (Ashton et al., 2012). They are essentially mitigating the effects of global climate change. Approximately 77% of all terrestrial above ground carbon stores are in the forests and also almost half of the total terrestrial gross primary productivity (GPP) are from tropical forests. Figure 1 shows the amount of world forest carbon stock via biome which also illustrates the high differences between each type of forest.

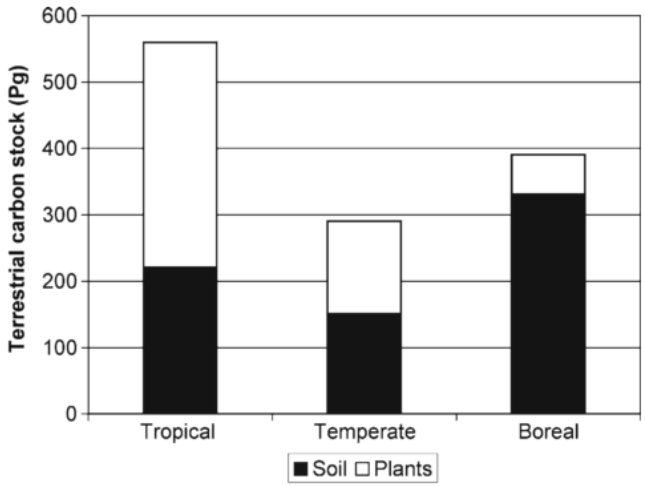

Figure 1 Distribution of world forest carbon stock representing by forest (Ashton et al., 2012)

Seventeen percent of global CO2 emission (annually) is attributed to land use and land use changes, especially from deforestation and forest degradation in the tropics (Ashton et al., 2012; Ciais et al., 2013). Hence, the study to reduce the amount of deforestation in the tropics is essential. In addition to that, study of the carbon fluxes in forests can also be conducted to inspect the amount of above ground carbon for future planning, as such measurements for tropical forest are very scarce (Pan et al., 2011).

In recent years, the United Nation Framework Convention on Climate Change (UNFCCC), an international environment treaty with near universal membership (Nuttall, 2015), has released an inducement policy of "Reducing Emissions from Deforestation and Forest Degradation" (REDD+). This policy occurred under the idea of payment for environmental services, particularly carbon payment for forest management in a sustainable way such that

biomass level increases (Bhattarai & Skutsh, 2015). The scale of accounted carbon has been addressed at three levels: i) *national* level (Chen, 2015; Cihlar et al., 2003), ii) *project* level and iii) a nested approach which is the combination of the first two levels (Angelsen & Atmadja, 2008). The project level approach has been found to be the most accurate and precise approach due to the method's reliance on field measurements (Bhattarai & Skutsh, 2015). Following this path of study to assess biomass and carbon pools will add more information of specific locations available to the world of research.

1.2. Overview of techniques for forest carbon estimation

For the estimation of forest carbon, there are four different sources of carbon to be measured: 1. Above ground biomass (AGB) which stands for all biomass in living vegetation above the soil, 2. Below ground biomass (BGB), the direct measurement of default root to shoot ratio, 3. Dead organic matter (DOM) concerns the deadwood and floor litter and 4. Soil organic carbon (SOC) which uses three major variables: soil depth, soil bulk density and concentrations of organic carbon for the estimation. The measurement of BGB is considered to be a very expensive, destructive and time consuming method while the SOC has the time component that requires to be taken in to consideration due to the slow change in soil. Although DOM uses the same field sampling method as AGB but it is not much popular. Considering that AGB is the only method seen by human eyes as well as remotely sensed data, this turned out to be the most effective method (Aalde et al., 2006; Bhattarai & Skutsh, 2015; Ravindranath & Ostwald, 2008).

The AGB measurement consists of plot method, harvest method, modelling, plotless or transect method, carbon flux measurement and remote sensing method. Firstly, the *plot method* or *field sampling method* is very common to find forest inventories variables like diameter at breast height (DBH) and height of the trees and apply these parameters in allometric equations. Secondly, *the harvest method* is the most accurate way of AGB estimation but, on the other hand, very costly. Next, *the modelling* is popular to estimate carbon stock for plantation project and used as a complement for field sampling method. Then, *the transect method,* which involves tree density and DBH series, is not suitable for dense vegetation. *The carbon flux measurement* has to create a chamber to observe several processes of CO_2 exchange. This method gives high accuracy but very expensive at the same time. . Lastly, remote sensing method, is very useful for large area but the issue to be considered is the resolution of satellite images and accuracy. Although the advanced technologies like Light Detection and Ranging (LiDAR) and Radio Detection and Ranging (RADAR) give a very proficient estimation, it also require advanced technical skills (Bhattarai & Skutsh, 2015).

Due to UNFCCC, one of the challenging tasks to retrieve the information of local forest carbon stock is the system to accurately and sufficiently assess the changes. A “sound and transparent measurement, reporting and verification“ or “MRV” system were created to response this challenge by using remote sensing techniques (Bhattarai & Skutsh, 2015). Remote sensing techniques which use the remotely sensed data to generate specific information for targeted application (Wulder & Franklin, 2003) such as in forestry have a lot of studies based on each platform, satellite, Synthetic Aperture Radar (SAR) (Kugler et al., 2015), aerial photograph which has been used as a main sources for forestry information especially the assessment of natural resources (Hall, 2003), LiDAR (Chen, 2015; Kato et al., 2014) or small platform like Unmanned Air vehicle (UAV) (Paneque-Gálvez et al., 2014).

Another study that uses the fusion technique to support other data is the study of Li et al. (2015) that integrated ALS data with SPOT-6 satellite data by geostatistical modelling. This study

aimed at the estimation of two inventory variables: forest canopy cover (CC) and AGB. The modelling workflow presented the solution for taking full advantages of sparsely collected LiDAR data and fulfilled the condition with satellite data within the geostatistical perspective.

Due to the sensitivity and low accuracy of conventional remote sensors in AGB estimation, along with the result in two dimensions images, newer technology like LiDAR has been developed to present the third dimension structure and higher accuracy in this field of study (Lefsky et al., 2002). Moreover, LiDAR can give higher resolution and 3D modelling of basal area and tree height with high precision, similar to 3D image matching technique that also estimate trees parameters in a less costly price.

1.3. Light Detection and Ranging (LiDAR)

LiDAR is an active sensor which directly derive 3D information of Earth's topography, vegetation characteristic and man-made construction (Renslow, 2012). In simple, LiDAR measures the distance between the sensor and a target surface by calculating elapse time between a short laser pulse emission and the return signals and multiply with the speed of light (Lefsky et al., 2002). LiDAR is used extensively in the forestry application with, the use of 3D point cloud derived from laser scanning to analyse biophysical attributes of trees (Liang et al., 2015).

LiDAR has four different types of measurement: airborne laser scanning (ALS), terrestrial laser scanning (TLS), mobile laser scanning (MLS) and the latest one, personal laser scanning (PLS) (Liang et al., 2015). Among these, ALS is the most common method in all field and especially for generating high quality digital elevation model (DEM). It can be done from a fixed wing aircraft or a helicopter (Vosselman & Maas, 2010). Figure 2 shows how the laser scanner works with airborne platform.

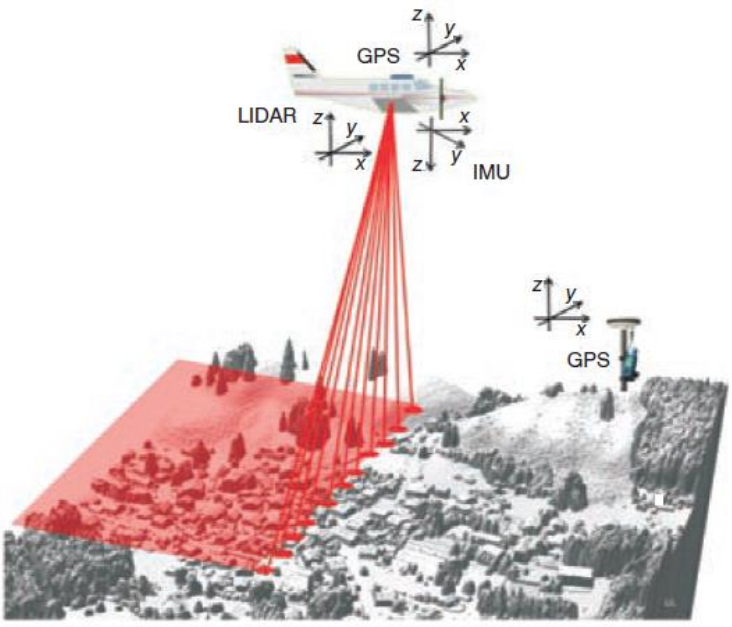

Figure 2 Airborne laser scanning principle (Vosselman & Maas, 2010).

The basic elements in ALS constitute of, airborne GPS antenna, Inertial measurement unit (IMU), control and data recording unit, operator laptop and flight management system (Vosselman & Maas, 2010).

In forestry application, ALS has been widely used due to the method's ability to penetrate through vertical trees structure. There is a rule of thumb to ensure that a forest is suitable to be

studied with ALS or not, by simply walk through the forest under the canopy and if a person is able to see the sky, it means that the ALS can also be used for that forest (Renslow, 2012). To begin with, Figure 3 shows the operation between laser pulses and tree canopy.

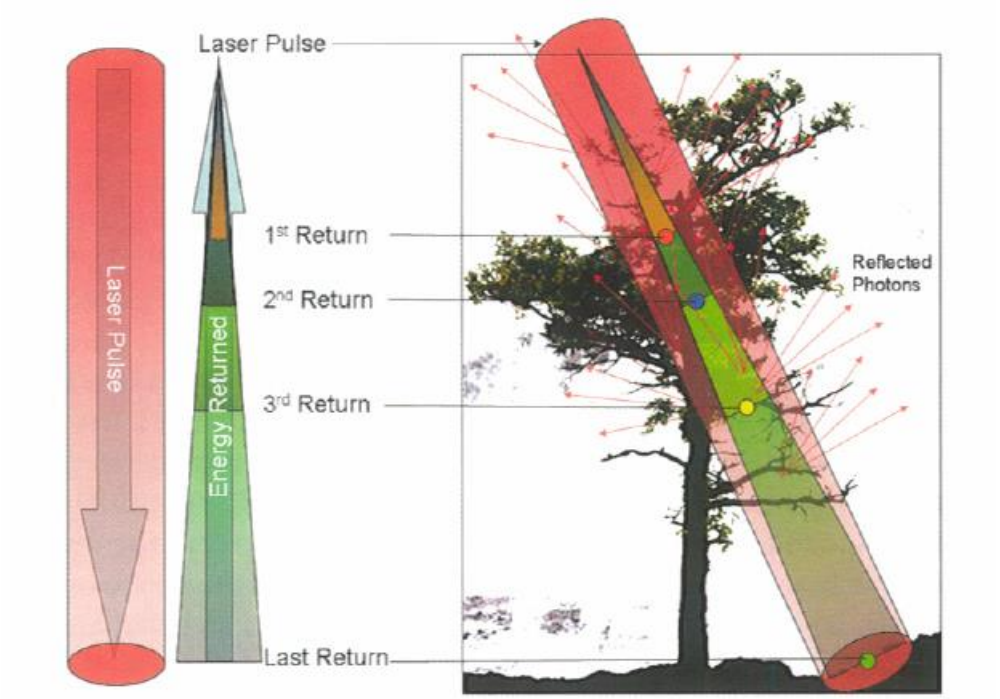

Figure 3 an example LiDAR pulse, interact with a tree and showing multiple returns (Renslow, 2012)

The laser pulse will interact first with the tree canopy and continue through to the ground below and reflects back the distance from target surface to the sensor. Furthermore, the result from this technique are 3D point cloud information of digital elevation model (DEM), digital surface model (DSM) and also the height of the canopy or crown height model (CHM) which is the difference between DEM and DSM. Other information derived from LiDAR are crown cover, forest structure, crown canopy profile and after post processing of LiDAR information, the results are expanded to have canopy geometric volume, biomass, crown dimensions and density (Mursa, 2013).

1.4. 3D Image-based matching point clouds

The long-time challenged research area is the 3D shape acquisition on stereo vision system, which is similar to human visual system and also automatic processes of 3D capture, analysing and visualization. The Two fields of study that are very close to each other are stereophotogrammetry and computer vision (Pears et al., 2012).

The word "photogrammetry" means the utilization of the measurement taken from two dimension images to retrieve three dimension coordinates of points on one's object (Mitchell, 2007). While the method of stereophotogrammetry is optimized with passive multiple images. This technique use the parallax principle of two different perspectives in different images looking at the same object or the common points. The intersection of two points of view is calculated using triangulation and the result is given in three-dimension location. This technique tends to mimic

normal human vision (Mitchell, 2007; White et al., 2013). The products derived from the photogrammetric workflows are height model, orthorectified images, 3D information etc.

The main advantages of image-based technique are cost effectiveness and easier acquisition of numerous overlapping images compared to LiDAR. On the other hand, image-based 3D point cloud generated by stereophotogrammetry cannot be used to extract DEM because optical images cannot penetrate through the gap of canopy as LiDAR does. For this reason, only upper canopy data will be extracted. Moreover, the effects from optical images that can cause errors to the matching technique are stereo-matching parameters, image resolution and sun angle difference. These characteristic affects the quality of both image-based point clouds and DSMs (White et al., 2013).

The manual method of stereophotogrammetry have been used in forestry for more than 65 years (White et al., 2013). After the evolution of computer technology and the automatic processing of stereophotogrammetry, this technique have been commonly used in many fields. The imageries were captured from different platforms for instance, airborne images (Ginzler & Hobi, 2015), Unmanned Air Vehicle (UAV) (Vetrivel et al., 2015) or even regular personal hand hold camera (Liang et al., 2015).

1.5. Problem statement

Due to the importance of forests as a significant source of carbon, the studies related to carbon estimation in forests have been plentifully researched. The use of carbon or biomass estimation – as an information to support and plan the policies in national level – is also a critical issue. The utilization of monitoring, reporting and verifying (MRV) to ensure the consistency in national approach is favourable for most nations (Angelsen & Atmadja, 2008). Though, the study in national level has a lot of errors compared to local scales (Chen, 2015). While, the project level has limited scope to study forests and also has close connection with the emission reduction. Consequently, REDD project can engage this project level when the countries are not ready to implement REDD method at their national level (Angelsen & Atmadja, 2008).

Lubowski, (2008) indicated that decreasing of emissions from tropical forests may provide an instant opportunity to mitigate an emissions source at relatively low estimated cost. Furthermore, Bhattarai & Skutsh, (2015) also mentioned that the carbon stock in the tropical rainforest even from other part than the tree – which normally stand for the largest proportion of total biomass in the forest – exceed the amount of carbon in the savannah woodland trees.

Moreover, MRV system has been using remote sensing techniques to improve its effectiveness and efficiency (Bhattarai & Skutsh, 2015). Besides, the potential of LiDAR to observe forest parameters is apparent despite the complexity of the tropical forest (Ashton et al., 2012). Furthermore, an advanced processing technique of digital airborne imagery to create image-based point clouds got more and more interest these days. Due to the availability of improved computers, the analyses of 3D data become significantly faster in recent days, making the former technology popular again to retrieve 3D information. Regarding the expenses, the cost of image-based method is just around 33 -50 % of the LiDAR method (White et al., 2013).

To examine the better approach of deriving biophysical factors of the trees and as canopy height and cover are the simplest parameters gained from canopy structure measurement (Lefsky et al., 2002). This study will focus more on the tree height, crown surface and crown height from both methods namely 3D image-based from aerial photo and airborne LiDAR. Furthermore, forest tree height is an important parameter for study timber production and has been used to estimate AGB and carbon flux measurements (Kugler et al., 2015). The utilization of remote sensing

techniques such as LiDAR to estimate tree height is assumed to be better than ground based estimation (Bhattarai & Skutsh, 2015). In addition, a study of White et al. (2013) claimed that both techniques are able to generate the canopy height with similar levels of accuracy. Hence, the comparison study of point clouds effectiveness between these two techniques in forest inventory variables may help further studies to select the appropriate acquiring techniques for each inventory factors.

Proving the relationship between LiDAR and ground measurement of corresponding forest attributes has been difficult in tropical forest due to the forest structure (Lim et al., 2003). However, study this complex structure from 3D point cloud with another technique like stereophotogrammetry of aerial photo can also be proved with LiDAR 3D point cloud information which can be counted as the highest accurate platform. The Structure from Motion (SfM) approach is not only facilitates the process of getting 3D point clouds in high accuracy from photographs (Fonstad et al., 2013), this automated techniques also gives the high spatial resolution 3D point clouds in the same level of point clouds derived from airborne LiDAR(Ota et al., 2015).

From all aforementioned, the study of assessing 3D point cloud from airborne LiDAR and image-based method in tropical rainforest of Ayer Hitam, Malaysia was proposed.

1.6. Research objectives

To compare the quality of 3D point clouds from image matching method and airborne LiDAR in tropical rainforest reserve of Ayer Hitam, Malaysia for potential carbon study.

1.6.1. Specific objectives

1. To compare the accuracy of trees height derived from 3D Image-based point clouds of aerial photo and airborne LiDAR.
2. To compare the accuracy of trees crown surface derived from 3D Image-based point clouds of aerial photo and airborne LiDAR.
3. To assess the accuracy of point clouds derived from 3D Image-based point clouds and airborne LiDAR by point-to-point method.
4. To compare the accuracy of crown height derived from 3D Image-based point clouds of aerial photo and airborne LiDAR.

1.7. Research questions

1. How accurate are the trees height derived from Image-based point clouds compare to the height from airborne LiDAR?
2. How accurate are the trees crown surface derived from Image-based point clouds compare to airborne LiDAR information?
3. How accurate are the point clouds from Image-based matching method and airborne LiDAR would be in point-to-point method?
4. How accurate are the trees crown height derived from Image-based point clouds compare to airborne LiDAR information in complex layers of tropical rainforest?

1.8. Research hypotheses

1. H_0: The trees height derived from Image-based point clouds is not significantly different from the trees height from airborne LiDAR
   H_1: The trees height derived from Image-based point clouds is significantly different from the trees height from airborne LiDAR

2. H_0: The trees crown surface derived from Image-based point clouds is not significantly different from the trees crown surface from airborne LiDAR
   H_1: The trees crown surface derived from Image-based point clouds is significantly different from the trees crown surface from airborne LiDAR
3. H_0: The trees crown height derived from Image-based point clouds is not significantly different from the trees crown height from airborne LiDAR
   H_1: The trees crown height derived from Image-based point clouds is significantly different from the trees crown height from airborne LiDAR

2. STUDY AREA AND MATERIALS

2.1. Study area

The Ayer Hitam forest reserve (AHFR) is situated in the Selangor state in Peninsular Malaysia at Latitude of 2°56'N - 3°16'N and Longitude of 101°30'E - 101°46'E (See Figure 4). This forest is a logged-over tropical rainforest and serves as an education and research site of University Putra Malaysia (UPM). In 1906 AHFR covered around 4,270 hectare but due to socioeconomic development (housing, oil palm plantations, new townships, factories and highway) the area is 1,248 hectare at present and is completely surrounded by build-up areas. The mean temperature is 27.8 °C while the lowest and the highest temperature are 24.6°C and 32.6°C respectively. The total annual rainfall in 1999 was around 3,300 millimetres (Ismail & Mohamed, 2008). Due to the urban surrounding of the forest, the biodiversity of Ayer Hitam forest is reduced. However, Lepun et al., (2007) claimed that the number of trees (DBH more than 5 cm.) in a 5-ha plot was 6,621 belonging to 50 families, 148 genera and 319 species. In addition, the study showed that 74% of the trees had a DBH between 0 and 14.9 cm, 23% of the trees had a DBH ranging from 15 - 44.9 cm and only 3% had a DBH larger than 45 cm.

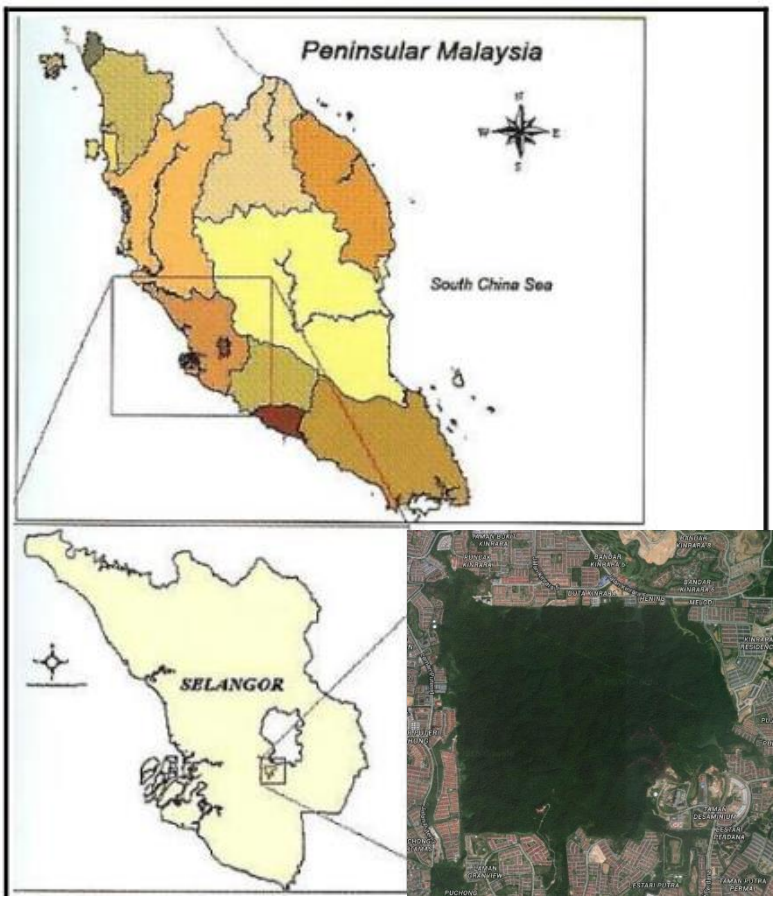

Figure 4 Map of Ayer Hitam Forest Reserve in Puchong, Malaysia, adapted from Ismail & Mohamed, (2008)

2.2. Materials

2.2.1. Data

The dataset was provided by the Faculty of Forestry, University Putra Malaysia (UPM), the partner university during the fieldwork. The dataset included raw data and ready-to-use data. The raw data where the aerial photographs, while the ready-to-use data comprised of airborne LiDAR (point clouds) data and the processed orthophotos. The point clouds data were recorded with the airborne LiDAR system LiteMapper 5600 in 2013 (see specification in

Table 1) and the aerial photos were taken with the DigiCAM-H or Hasselblad camera in 2011 (see the specification in Table 2). The spatial resolution of aerial photos were 13 centimetres. The density of the point cloud of the airborne LiDAR was around 5 - 6 points per square meters.

Table 1 the major technical parameters of the LiteMapper 5600 system

Pulse rate	Range between 70 kHz and 240 kHz (normal 70 kHz)
Scan angle	60°
Scan pattern	Regular
Effective rate	46,667 Hz
Beam divergence	0.5 mrad
Line/sec	Max 160
A/c ground speed	90 kts
Target reflectivity	Min 20% max 60% (vegetation 30%, cliff 60%)
Flying height	700 m–1000 m
Laser points/m2	0.9 to 1.2 points with swath width 808 m to 1155 m
Spot diameter (laser)	0.35 to 0.50 m
Max (above ground level)	1040 m (3411ft)

Table 2 the specification of the DigiCAM-H (Hasselblad camera)

Pixel size	6.8 µm
Sensor size	36.8mm x 49.07mm: true size of the internal sensor
Image size	7216 x 5412 pixels (39mp)
Lens: Focal length	50 mm
Max aperture	3.5
Forward cross track	52°
Forward along track	40°
Flying height	600 m at mean sea level

2.2.2. Software

The software used in this study is listed in Table 3. Several software were used as a part of the study. A complete list of these software was shown in Table 3.

Table 3 list of software used in the study

No.	Software	Purpose
1.	PIX4D (supported by RTAF)	Bundle block adjustment/ 3D Image-based matching/Point cloud generation
2.	LAS Tool	Point cloud processing
3.	Cloud compare	Point cloud processing and analysis /accuracy assessment
4.	Erdas Imagine 2015	Image processing
5.	Arc Map 10.2.2	GIS analysis/ Back-engineering
6.	R studio/ R	Back-engineering/ Statistical analysis
7.	Microsoft Word/ Excel/ Power Point/ Visio/ Project/ Adobe Acrobat Reader DC	Writing and presentation
8.	Mendeley Desktop	Referencing

2.3. Sampling methods

83 individual trees were selected randomly from all datasets. Thus, simple random sampling was used as a sampling method in the study.

3. METHODS

The overall study consisted of 3 broad sections: (i) data pre-processing, (ii) data processing and (iii) data analysis. An overview of the consecutive steps in the method is presented in the flowchart (see Figure 5). The following subchapters discusses the steps undertaken in each of these sections are provided in the flowchart below.

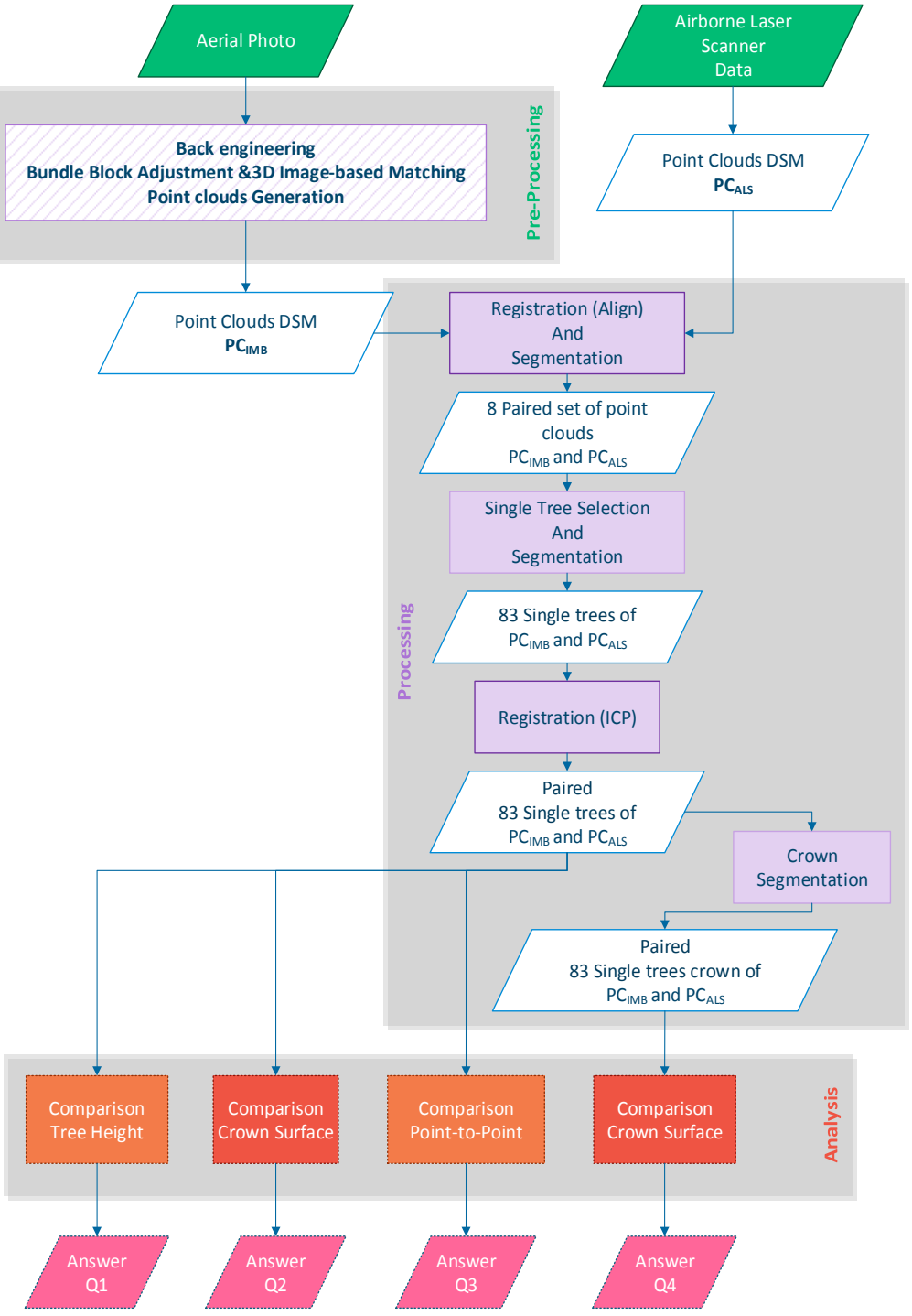

Figure 5 flowchart of method

3.1. Data Pre-Processing

Data Pre-Processing consisted of 3 steps: (i) the back-engineering of orthoimage map, (ii) bundle block adjustment & 3D image-based matching and (iii) point cloud generation.

The back-engineering of orthoimage map

Extraction of point clouds from aerial stereo images required the information regarding interior orientation, exterior orientation, camera calibration and central coordinates of each photographs. However, as the information about the central coordinates of each photographs were missing, a back-engineering process was carried out.

"Back-engineering" of orthoimage map is the process to the reconstruct coordinates of points in each aerial photograph by image matching techniques, by referring to the coordinates of the same point in the orthoimage map.

In this study an "R-script" was written to identify the center point of each aerial photograph (see Figure 6 and Figure 7). Thereafter, the coordinates of these center points were established by identifying the exact same spot on the orthophoto.

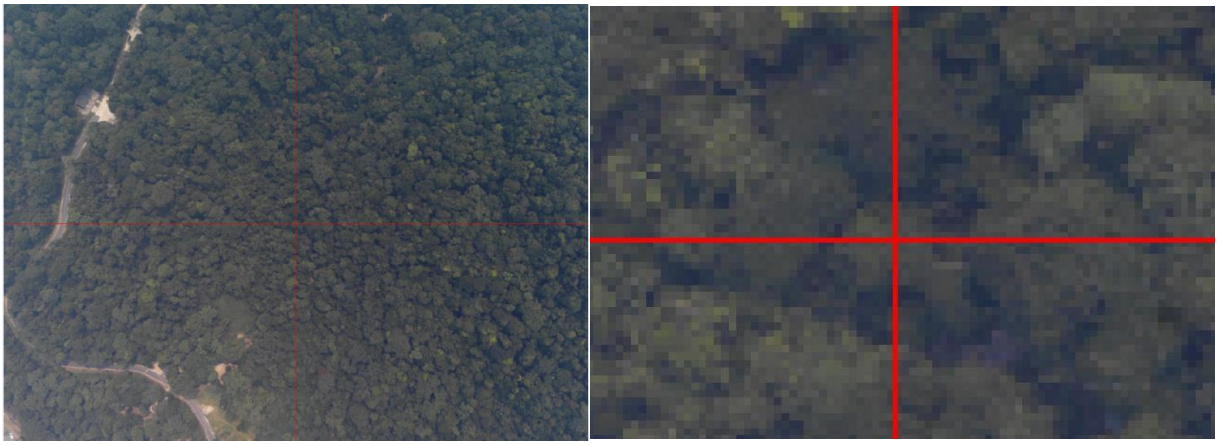

Figure 6 showing the cross line in an aerial photo to define the centre point of the image. The image in the left shows the overview and the right hand image zooms in to a detail level that allows identification of the same spot on the orthophoto

```
j<-0

for (i in 1:479){
j<-j+3
AyerHitamCentreAerial_brick_temporal<-stack(AyerHitamCentreAerial[[j-2]],AyerHitamCentreAerial[[j-1]],AyerHitamCentreAerial[[j]])
jpeg(paste(name[i],"_MID.jpg",sep=""),width=7216,height=5412)
plotRGB(AyerHitamCentreAerial_brick_temporal)
abline(h=2706, col="red",lwd=5)
abline(v=3608, col="red",lwd=5)
dev.off()
}
```

Figure 7 R script for defining the center point in each aerial photo

Bundle block adjustment & 3D image-based matching

The process of Bundle block adjustment is based on the collinearity equations that calculates all the image parameters like interior orientation, exterior orientation, camera calibration, and central coordinates. The calculations are based on the position in the image and related to ground control points. (Katoch, 2013; Linder, 2009). The unavailability of ground control points has led the study to adopt manually generated ground control points (or in this case called MTPs: Manual Tie Points) using physical features which can be easily identifiable and matched with the orthoimage map.

The 3D image based matching or structure-from-motion, is the process of generating 3D points based on 2D images. In case of this study, the 2D images have the X, Y values (location), and this process generated the Z value which represented the height. Chapter 1.4 discussed this technique in more details.

The study used Pix4D programme provided by Royal Thai Air Force (RTAF) to execute these processes. The estimated Ground Sampling Distance (GSD) is calculated from camera sensor size, image size, focal length and flying height from Table 2 (see Equation 1).

Equation 1: Ground Sampling Distance (GSD) calculation

$$\frac{S_w \times H \times 100}{F_R \times imW}$$

When; S_w = the sensor width (mm)
H = the flying height (m)
F_R = the focal length (mm)
imW = the image width (pixel), (PIX4D, 2016b)

The coordinates obtained from the back-engineering processes were utilized as a geo referenced information in every single aerial photograph. All 352 aerial photos and their coordinates, together with camera orientation information were entered.

The software Pix4D requires selection of several parameters (Table 4) in order to run bundle block adjustment and 3D image-based matching. In this study, the default settings were kept for all parameters, except number of neighbouring images and MTPs. These values were selected through a "trial and error" method and the values that provided the best result were used for the parameters.

Table 4 settings of bundle block adjustment and image matching in Pix4D software

Processing Options	Setting
Image Scale	0.5
Number of Neighbouring Images	4
Use Triangulation of Image Geolocation	Yes
Use Image Similarity	Yes
Use MTPs (Manual Tie Points)	Yes
Maximum Number of Image pairs per MTP	50
Use Geometrically Verified Matching	Yes
Calibration Method	Standard
Internal Parameters Optimization	All
External Parameters Optimization	All
Rematch	Yes

Point cloud generation

The point clouds datasets were generated using the Pix4D software. Some of the studies used this software to generate point clouds (Hernández-clemente et al., 2014; Vetrivel et al., 2015). The software settings applied are listed in Table 5.

Table 5 the settings for both high density and optimal density options

Setting	High Density	Optimal Density
Image Scale	Multiscale, ½ Image Size	Multiscale, ½ Image Size
Minimum Number of Matches	2	2
Matching Window	7x7 Pixels	7x7 Pixels

The Pix4D programme provides two options of point cloud generation; i) high density and ii) optimal density. The settings for "matching number" was set to 2, due to the very low overlap area of the aerial photographs and to maximise the number of resulting points same as in the study of St-Onge, Audet, & Bégin, 2015.

The software allows the generation of two types of point clouds: optimal density and high density. Both options were evaluated in order to determine which one was appropriate for comparison with the ALS point cloud (see section 4.1 Results of point clouds generation).

3.2. Data Processing

The point clouds generated from aerial photos have their own natural colour (RGB) while the point clouds from ALS have only a single colour. Colouring the ALS point clouds based on the Z value helped in the visual evaluation of the results. The data processing mainly focused on the point cloud processing which comprised of 4 steps: (i) registration (align) & segmentation, (ii) single tree selection & segmentation, (iii) registration (ICP) and (iv) crown segmentation.

Registration (Align) and Segmentation (1)

Registration (align) or so called "point pairs picking" was done with the help of CloudCompare software (Daniel, 2016). This is the method to make two sets of point cloud comparable. The method aligns the two different data sets on top of each other and calculates how accurately the points between the two data sets match. This type of registration allows the users to manually pick at least three corresponding points in both datasets which are point clouds derived from aerial photograph and the ALS and also select the reference dataset which is ALS in this case. After alignment, the program will reports the final RMS value for the each dataset.

The segmentation stage consisted of subdividing the dataset into a number subsets which are required for the next steps. The ALS point clouds (PC_{ALS}) consisted of 23 grid tiles, out of which 8 were selected for point clouds matching with image-based point clouds (PC_{IMB}) see Figure 8. In total, there are 8 subsets of both point clouds and 10 trees were randomly selected from each subsets plus 3 individual trees for further analysis.

Single Tree Selection and Segmentation (2)

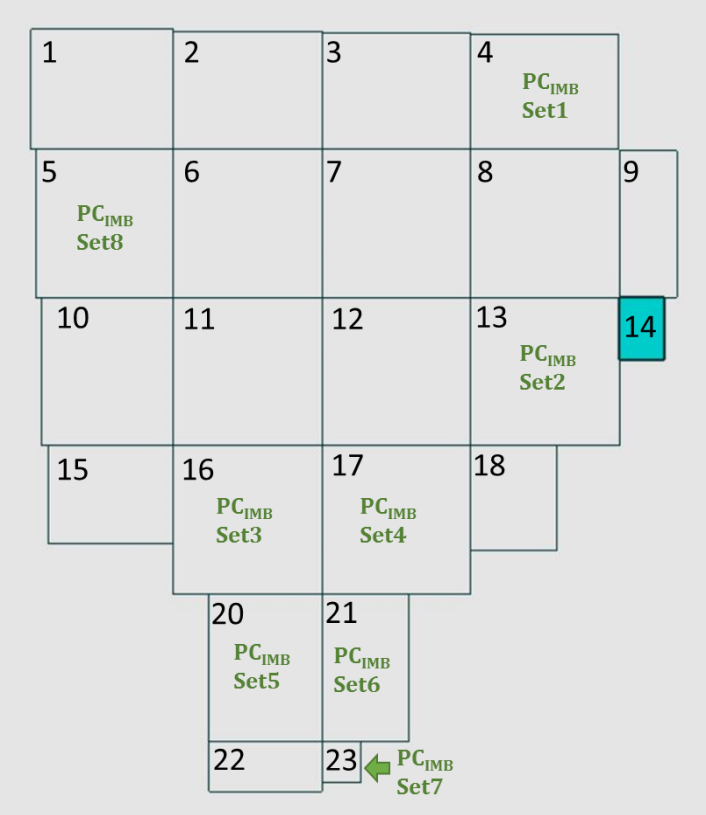

Figure 8 Point clouds matching and their subsets. The tile 1-23 are obtained from PC_{ALS} while set 1-8 are from PC_{IMB} and used for matching

The Tree Detection Model can be done in two approaches: (i) individual tree and (ii) area-based approach. As the area-based approach aggregates the value of the whole area to a mean value, in compare to single tree method which measures each tree individually, it may be less accurate. Considering this disadvantage of the area-based approach, the single tree detection was selected. Moreover, the first model is suitable for data with a point density greater than 3-5 points/ m^2, whereas the second model can be applied in larger areas with lower point density (Hollaus, 2015). Since the available data for this study has more than 5 points/ m^2, the single tree detection was selected. In each of the subsets described in the previous section, 10 trees were randomly selected for further analysis.

Furthermore, the segmentation was done by manual delineation of the selected trees in all subsets. The visual segmentation from top view were used to delineate tree crown separately.

Registration (ICP)

The fine registration (ICP)(Daniel, 2015b) in CloudCompare software uses the original ICP algorithm called "Iterative Closest Point"(Besl & McKay, 1992). The algorithm finds the closest point in local minimum of a mean-square metric of one dataset to another dataset in order to match or register these two sets more finely. After matching, the visualization will be better and easier to do further analysis.

Crown Segmentation

Crown segmentation is the process to cut the point clouds dataset from the previous steps. The segmentation left only the tree crown and removed out the under tree ground information. The visual analysis was used as an approach in Cloudcompare. See Figure 9 for more details about the definition of crown height.

3.3. Data Analysis

Before going to data analysis in each objectives, the following Figure 9 will describe the terms used in this study.

Figure 9 the terms used in this study: tree height, crown surface and crown height

. Most of the studies in LiDAR relied on the use of a digital surface model (DSM) in raster version, which is more suitable for larger areas. However, to study individual trees, the point cloud based method seems to be more appropriate. Point clouds contain an X, Y (location) and Z value (height) per point, as opposed to, the rasterized data, which provide coarser information in the form of a certain pixel size (determined by the researcher and depending on the point density of the original LiDAR data) with a Z-value based on an average of the highest and lowest value in that pixel(Koch et al., 2014). Thus, data can be missing if raster data was used to represent the amount of data within one cell. In this study, all the analysis is based on the point cloud.

R software package "rLiDAR" (Silva et al., 2015) was used to create data files in *.las format and compute the point clouds metrics (tree height and crown hight) and surface area (crown surface) of all 83 trees for tree height,.

For comparison of the point cloud derived from the aerial photographs and the LiDAR, the minimum, maximum and average tree and crown height and minimum, maximum and average crown surface were calculated. Moreover, the Root Mean Square Error and Normalized Root Mean Square Error were established (see Equation 2and Equation 3 respectively). The RMSE is expressed in meters or square meters and the NRMSE is expressed as a percentage. In order to test the hypothesis, a linear regression was carried out to determine the significance and the coefficient of determination (r^2).

Equation 2 RMSE calculation

$$RMSE = \sqrt{\frac{\sum(Y_1 - Y_2)^2}{n}}$$

Where; Y_1 = value from Airborne LiDAR data
Y_2 = value from 3D Image-based matching data
n = number of sample (83 trees)

Equation 3 NRMSE calculation

$$NRMSE = \frac{RMSE}{\bar{y}_1}$$

Where; RMSE is from Equation 2
$\bar{y}_1$ = mean value from Airborne LiDAR data

3.3.1. Tree height analysis

The functions "readLAS" and "rMetrics" from package 'rLiDAR' (Silva et al., 2015) were used as part of the R script to derive *.csv files of all 83 individual trees metrics (see example of tree number 1 in Figure 10). The tree height was calculated from the maximum and minimum height of the point cloud in both aerial photograph and LiDAR datasets.

```
# TRY with rMetrics of individual tree
tree1_als <- readLAS("000004 - ALS_tree1.las")
tree1_imgopt <- readLAS("352img_part_5UP - OPT_tree1.las")

tree1_metricsALS <- rMetrics(tree1_als)
tree1_metricsOPT <- rMetrics(tree1_imgopt)

tree1 <- as.data.frame(cbind(t(tree1_metricsALS),t(tree1_metricsOPT)))
names(tree1)<-c("tree1_metricsALS","tree1_metricsOPT")
write.table(t(tree1),"tree1.csv",row.names = FALSE)
```

Figure 10 R script to retrieve the tree height metrics

After creating *.csv file of all 83 individual trees, the descriptive statistics (mean, maximum and minimum) were calculated for tree height, along with the linear regression model , RMSE and r^2.

3.3.2. Tree crown surface analysis

For tree crown surface analysis, the functions "readLAS" and "chullLiDAR3D" from the same R package were used as part of the script to create another set of 83 *.csv files with the individual trees crown surface information.

```
#############chullLiDAR3D#############################
chullLiDAR3D(tree1_als, plotit = TRUE, col = "forestgreen", alpha = 0.8)
chullLiDAR3D(tree1_imgopt, plotit = TRUE, col = "forestgreen", alpha = 0.8)
chullLiDAR3D(tree2_als, plotit = TRUE, col = "forestgreen", alpha = 0.8)
chullLiDAR3D(tree2_imgopt, plotit = TRUE, col = "forestgreen", alpha = 0.8)
```

Figure 11 R script for retrieving crown surface information

From these files the descriptive statistics (mean, maximum and minimum crown surface) were calculated for tree height, along with the linear regression model, RMSE and r^2.

3.3.3. Point-to-point method

The "Point-to-point" or "cloud to cloud" method is a function to measure the distance of point pair set in a tree in "CloudCompare" software. In this case, the default settings were used. Meaning that the cloud to cloud distance is based on the nearest neighbor distance (Daniel, 2015a).

In line with the hypothesis, the PC_{ALS} acted as a reference while PC_{IMB} performed as the compared cloud. All distance of each point pairs were calculated relatively to the PC_{ALS} reference cloud. The smaller distance between the points, the better the comparability of the point clouds.

All 83 trees from PC_{ALS} and PC_{IMB} were compared one by one in "CloudCompare" software. The minimum, maximum and average distance were calculated between PC_{ALS} and PC_{IMB}. Moreover, the sigma (standard deviation) and maximum relative error are given.

3.3.4. Crown height analysis

Crown height or crown depth is length along the main axis from the treetop to the base of the crown (Zhang, Zhou, & Qiu, 2015). Due to the biodiversity and the complexity of the vegetation structure in the tropical rainforest (see Figure 12), observing the vertical structure of the forest helps a lot in the study of forest habitat quality assessment (Hollaus, 2015). Furthermore, the ALS can detect the ground layer through the gaps in the tree crowns and obtain DTM information. The 3D estimation from aerial photograph on the other hand can only detect the tree canopy. In this research the depth of the crown derived from the aerial photographs is compared with the same parameter derived from the ALS data set.

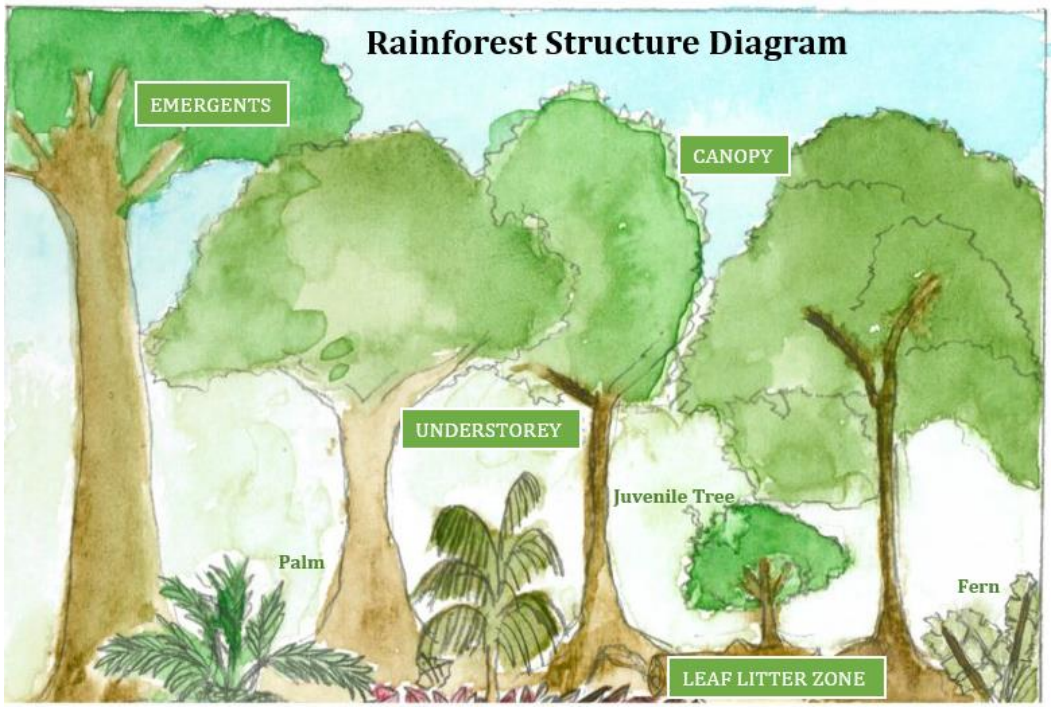

Figure 12 tropical rainforest structure diagram

The result of tree crown segmentation were used as an input for this analysis. The functions "readLAS" and "rMetrics" from package 'rLiDAR' (Silva et al., 2015) were used as part of the R script to derive *.csv files of all 83 individual trees crown metrics (see example of tree crown number 1 in Figure 13). The tree crown height was calculated from the maximum and minimum crown height of the point cloud in both aerial photograph and LiDAR datasets. The descriptive statistics (mean, maximum and minimum), the linear regression model, RMSE and r^2 were calculated.

```
##Script for rMetrics of individual crowns (83 trees)
# tree1
crown_tree1_als <- readLAS("ALS_crown_tree1.las")
crown_tree1_imb <- readLAS("IMB_crown_tree1.las")

crown_tree1_metricsALS <- rMetrics(crown_tree1_als)
crown_tree1_metricsIMB <- rMetrics(crown_tree1_imb)

tree1 <- as.data.frame(cbind(t(crown_tree1_metricsALS),t(crown_tree1_metricsIMB)))
names(tree1)<-c("crown_tree1_metricsALS","crown_tree1_metricsIMB")
write.table(t(tree1),"crown_tree1.csv",row.names = FALSE)
```

Figure 13 R script to retrieve the tree metrics for tree crown height

4. RESULTS

The results are divided into three sectors: (i) data pre-processing, (ii) data processing and (iii) data analysis.

4.1. Data Pre-Processing

The results from the Data Pre-Processing contains the result of back-engineering of the aerial photographs using the orthophoto , bundle block adjustment&3D image-based matching, point cloud generation and also the descriptive statistics of 83 individual trees.

The back-engineering of orthoimage map results

As mentioned before in section 3.1 "Data Pre-Processing", the back-engineering process at reconstructing the coordinates of the center points of the aerial photographs. The results shows that the flight lines in the left part of the study area are not straight (see Figure 14). Obviously this has an effect on the overlap and sidelap between consecutive images. Some aerial photos were missing and the incompleteness is particularly striking in the area around main office of AFHR (see red circle in Figure 14).

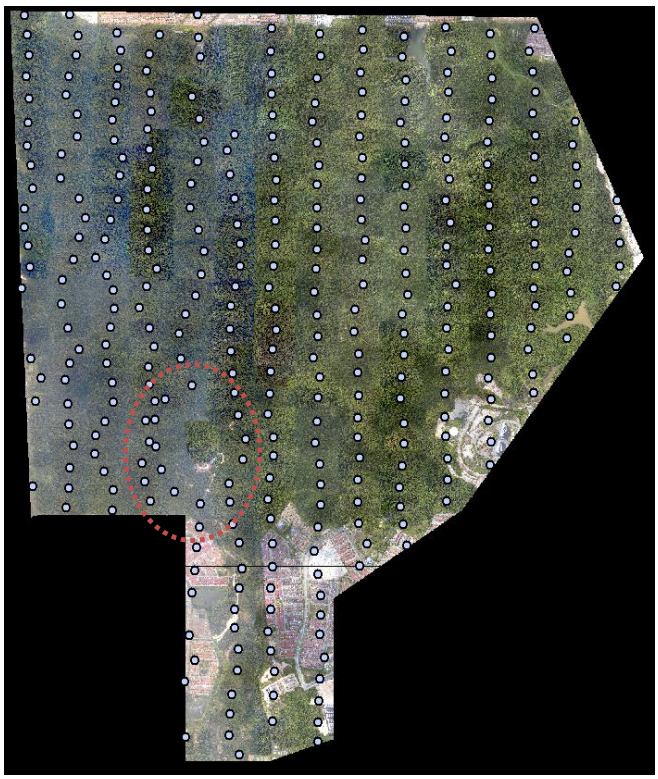

Figure 14 the centre points of aerial photos from back-engineering processes (blue dots) on top of orthoimage map

Bundle block adjustment & 3D image-based matching results

After running Pix4D program, a report was generated automatically. The average Ground Sampling Distance (GSD) result of this dataset is 6.24 centimeters and is comparable to the estimated GSD calculation in section 3.1 which was 6.12 centimeters per pixel. There are only 105

images calibrated out of 352 images because of the complexity of forest, the flight line distortion and image overlaps as illustrated in Figure 15.

Moreover, the missing aerial photos and reduced overlap area affected the bundle block adjustment and 3D image-based matching. The higher amount of aerial photos and the higher the overlap area, the better results will be of bundle block adjustment. For this step, the result covered the area of 5.6284 sq.km. That represents around 29% of the total area covered by the aerial photographs.

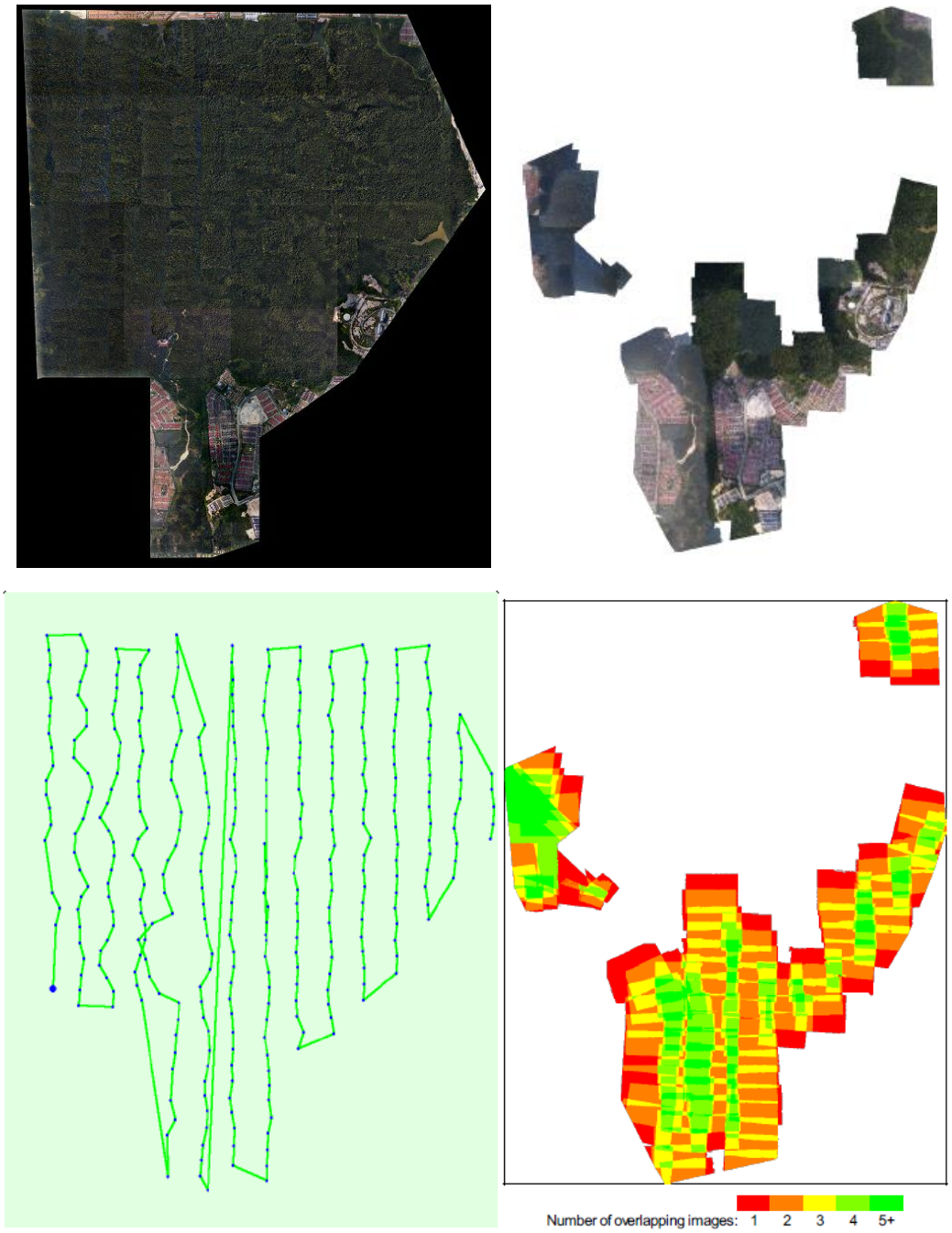

Figure 15 (top left) the orthoimage map obtained from UPM, covered the whole study area, (top right) the orthoimage map resulted from back-engineering coordinates and following processes, (lower left) line connected from dots represent the position of aerial photos which signify the flight line of the study area, (lower right) showing the number of overlapping images generated in this study.

Results of point clouds generation

The result in this step corresponded to the result from the previous step. As the point clouds generally generated from the overlap area of aerial photographs, the missing images affected the completeness of point clouds itself. Likewise, the generated image-based point clouds had the same area as the orthoimage map resulted from the previous stage (see Figure 15, top right). As mention in section 3.1 point cloud generation, in stage two point clouds were generated: optimal density and high density. Table 6 shows the results of this point cloud extraction, expressed as total number of 3D points extracted and the average density of the point cloud per m^3.

Table 6 showing two settings of different density datasets

Results	High Density	Optimal Density
Number of 3D Densified Points	257,989,774	71,025,304
Average Density (per m^3)	24.26	7.04

Since the ALS point cloud has a density of 5-6 points/m2, the optimal density point clouds derived from the aerial photographs is more comparable to the ALS than the high density data, even though the high density point clouds can "pick up" more from the objects in the study. The option to generate a denser point cloud does not necessarily mean better data. The program itself claims that increasing the density of the point clouds does not necessarily increase the quality of point clouds (PIX4D, 2016a). Furthermore, after comparing the preliminary result for point clouds selection, it turned out that the high density data systematically overestimated the height of the trees when compared to the ALS point clouds. The average difference of sample trees from both density's data are 48.52% and 38.93% for high and optimal density respectively (see appendix I). As a result, the optimal density result was chosen to use as an input data for the next steps.

In Figure 16, the illustration shows the chance to exactly hit the highest point of a tree using optimal density and ALS is much smaller compared to the high density option.

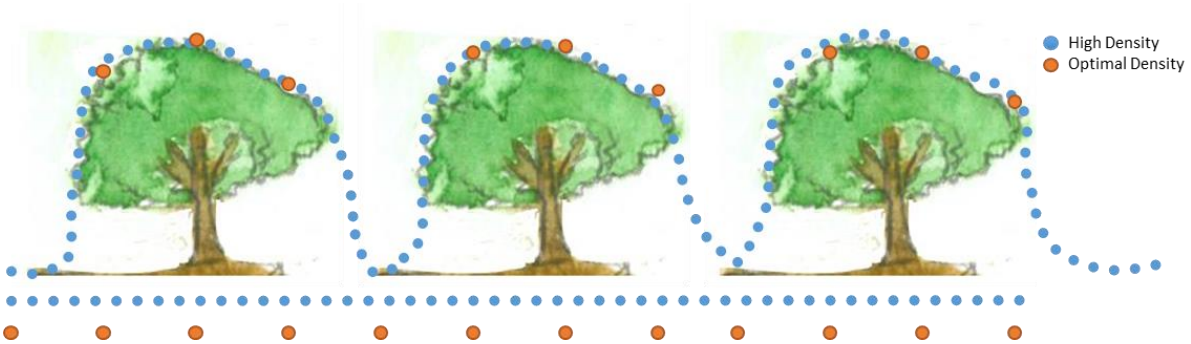

Figure 16 the difference of high and optimal density point clouds generated and the chance to pick up information in the real world situation.

4.2. Data Processing

Registration (Align) and Segmentation (1)

Figure 8 illustrates the selection of 8 subsets for point cloud matching resulted from the incompleteness of point clouds for the whole study area (see Figure 15 top right). Where Figure 17 shows an example of the results of point cloud matching which also referred to as align or point pair picking. This subset required at least 3 point pairs to do the point cloud matching, with a final RMS of 0.835. The other 7 subsets were registered and segmented in the same procedure.
Figure 17 also shows the registration of point clouds sets with 3 point pairs in the figure: R0, R1 and R2. These points were registered in the same point of both dataset.

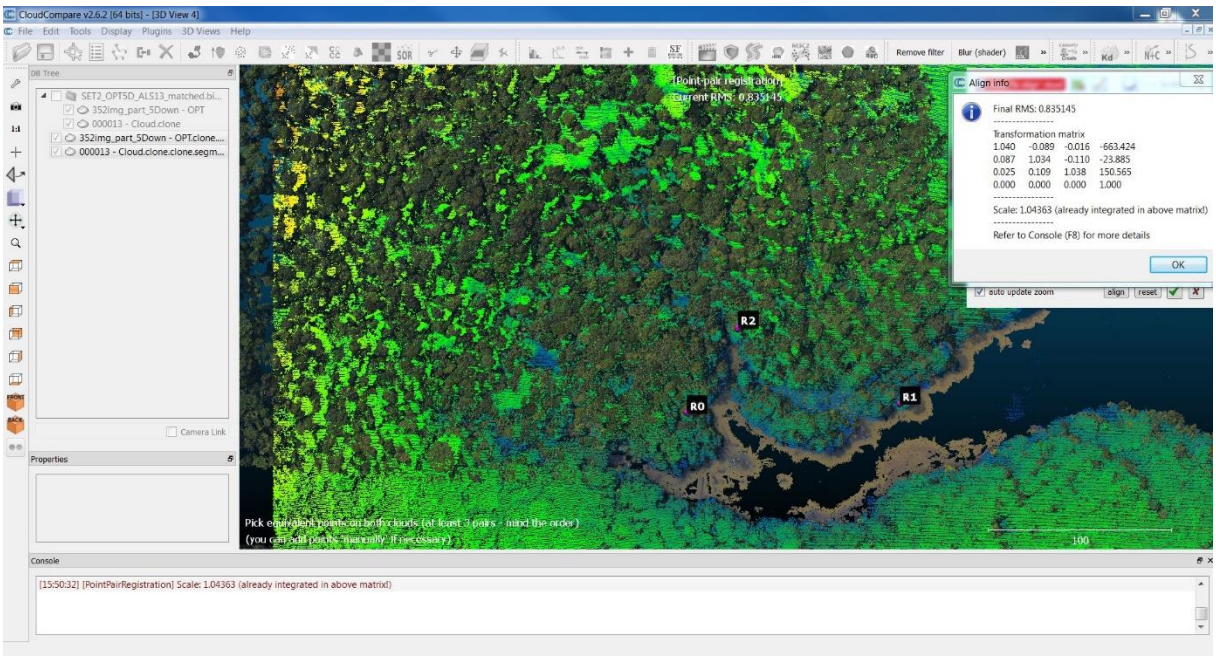

Figure 17 an example of the subset point clouds to be aligned using point pairs picking registration and its RMS error value

Single Tree Selection and Segmentation (2)

From 8 planned subsets of point clouds, 10 trees in each subset plus 3 additional trees were picked and segmented from the top view along the crown shape. The additional trees were intentionally used to compare with individual trees from the field but the data were not sufficient to compare. Thus, adding 3 more trees doesn't affect the study and also add the number of sample. Due to this, 83 trees were selected and segmented for further analysis. The information of each tree can be seen in Table 7.

Table 7 point clouds subsets and trees

Subset number	Tree number
1	1 – 10
2	11 – 20
3	71 – 80
4	21 – 30
5	61 – 70
6	31 - 40
7	41 – 50
8	51- 60

Figure 18 is an example of the manually digitized circumference (green circle) of a randomly selected tree in one of the subsets. This process was repeated for each of the 83 trees.

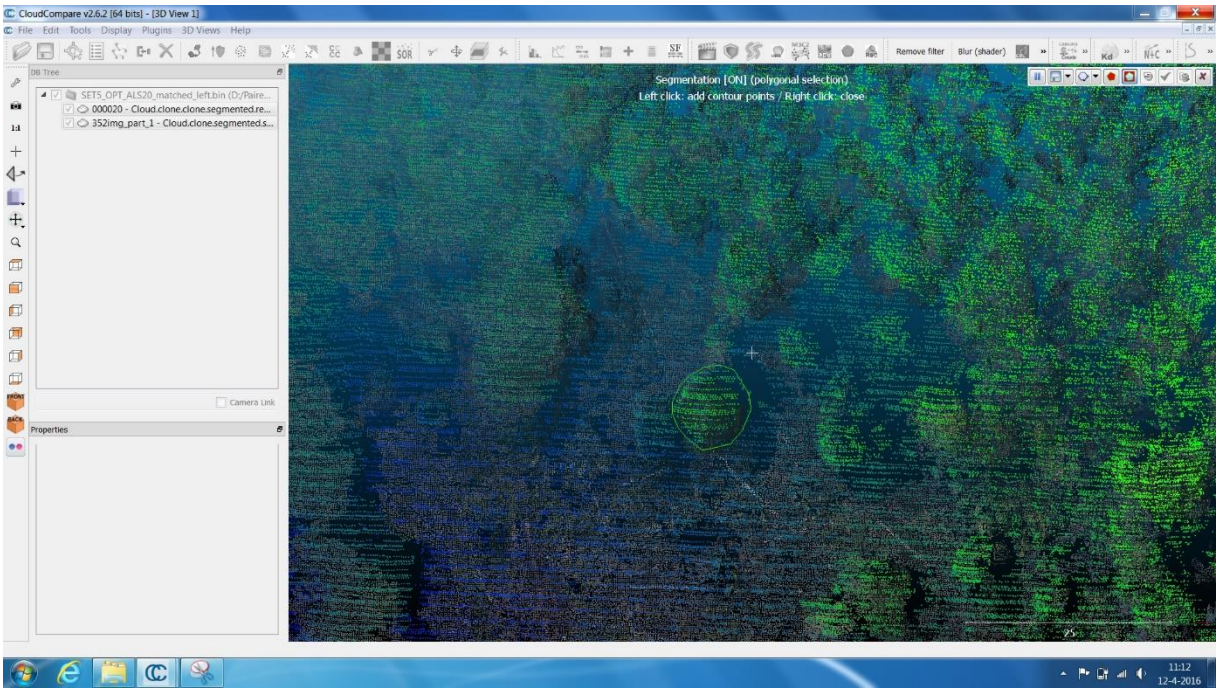

Figure 18 the single tree selection and segmentation was performed and displayed in the green circle area

Registration (ICP)

The ICP registration was done one by one for all 83 trees in the PC_{IMB} data set, using PC_{ALS} as a reference data source. After registration a visual inspection was carried out to assess if the point clouds matched, from 4 viewpoints including front, back, left and right side. In the example of ICP registration in Figure 19, the green dots denote PC_{ALS} while the darker green dots are of PC_{IMB}. The left side of the figure shows the two point clouds before registration and the right hand side image show the results after registration. It is clear that the points in the PC_{IMB} point cloud moved to match to the corresponding points in the PC_{ALS} point cloud.

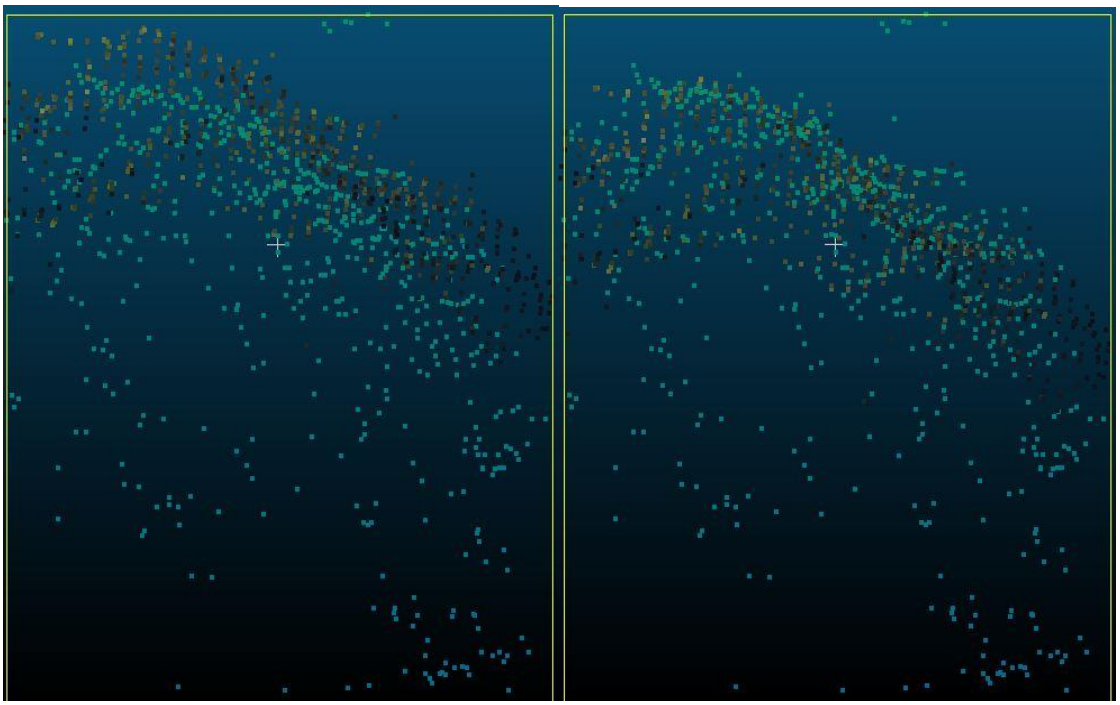

Figure 19 individual tree number 22 before ICP matching (left) and after ICP matching (right)

Crown Segmentation

The crown segmentation was done for the further analysis of tree crown height. A group of point clouds representing ground information under the trees were removed. The yellow box in Figure 20 signifies the groups of points that planned to be cut. The results left in this stage were

the part of tree crown only. After doing this segmentation for the whole dataset, the result are 83 individual tree crowns.

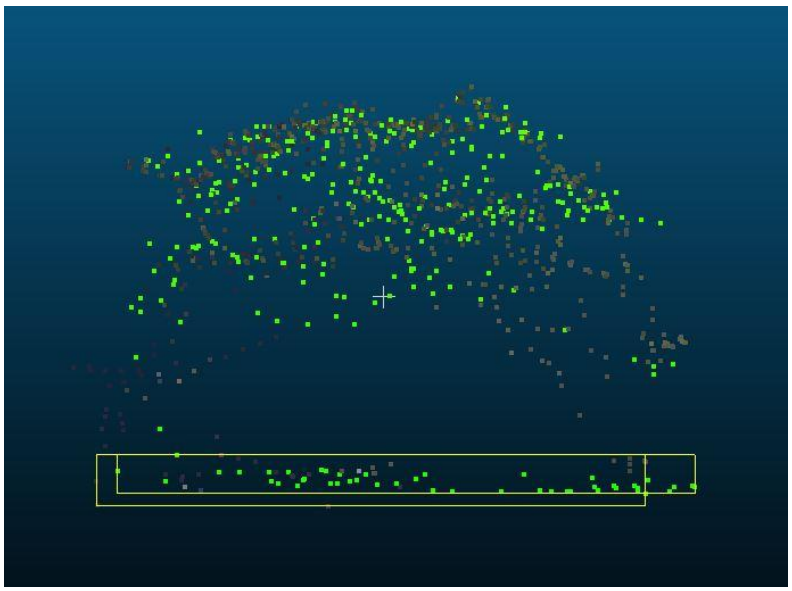

Figure 20 crown segmentation for crown height analysis. The light green points represented PCALS and the dark green points represented PCIMB. The yellow rectangle showed the groups of points that were going to be cut out

4.3. Data Analysis

Next to the summary of descriptive statistics, the RMSE and NRMSE, a linear regression model is given for each of the objectives. The data for tree height, crown surface, and crown height per individual tree, and point-to-point distance between PC_{ALS} and PC_{IMB} are given in appendix II to V.

4.3.1. Comparison of tree height from 3D Image-based matching method and Airborne LiDAR

The tree height from aerial photos and ALS were matched in form of point clouds based method for all 83 trees. To summarize, the descriptive statistics for all tree height displays in Table 8.

Table 8 the results of comparing tree height from 3D Image-based matching method and airborne LiDAR

Minimum Difference in Meters	Maximum Difference in Meters	Average Difference in Meters	Minimum Difference in %	Maximum Difference in %	Average Difference in %
0.03	29.75	5.87	0.13	77.63	24.91

The RMSE value between two datasets for tree height is 9.48 meters and the NRMSE value is 0.479 or 47.9%

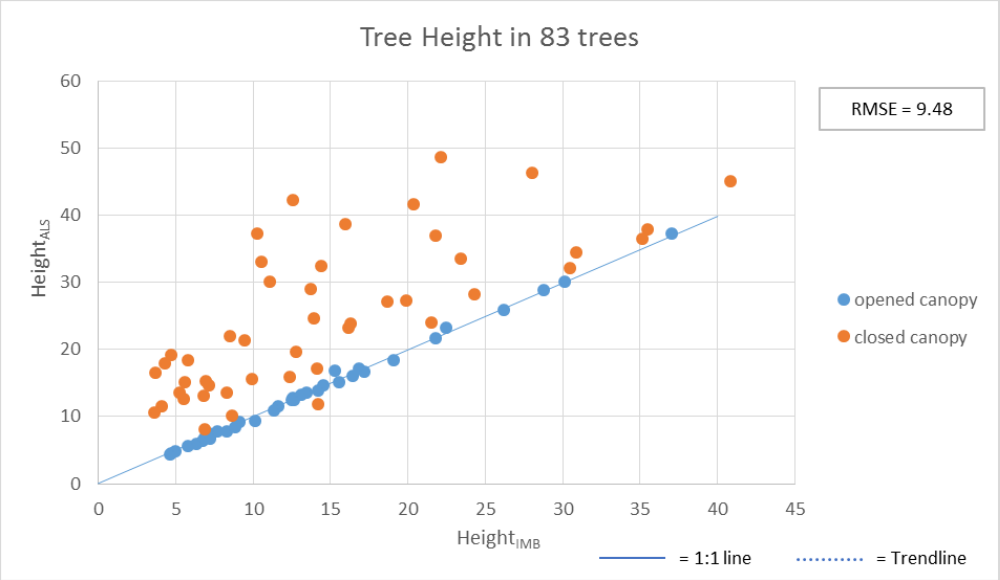

Figure 21 linear regression model of tree height from 3D Image-based point clouds and Airborne LiDAR with trend line and 1:1 line

Table 9 summary of regression statistics output for tree height comparison

Regression Statistics output	
R squared	0.54
Adjust R Squared	0.53
Standard Error	7.70
df	81
F-statistic	96.96
p-value	1.69e-15

The equation obtained from the linear regression is:

Equation 4 tree height equation from regression model

$$Height_{ALS} = (0.9645 \times Height_{IMB}) + 6.1455$$

Where, $Height_{IMB}$ = Height value from Image-based point clouds
And $Height_{ALS}$ = Height value from Airborne LiDAR; all unit is in meter.

Some points in the graph in figure 21 fitted very well on the 1:1 line. Meaning that the match between two datasets is optimal. These points concern "stand-alone trees" close to the village, road and forest border. Points far away from the 1:1 line concern trees in dense forest. In these situations only the ALS provides elevation information of the forest floor, since it can "pierce through" gaps in the canopy, while image-based point clouds mainly provide data from the canopy. This also accounts for the fact that the image-based point clouds tend to under estimate the height (nearly all the deviations lie under the 1:1 line).

The hypothesis to be tested for this research question is:

H_0: The trees height derived from Image-based point clouds is not significantly different from the trees height from airborne LiDAR

Only in the case of solitary trees and trees in a part of the forest with an opened canopy, the null hypothesis cannot be rejected, which means there is no significant difference between the tree height measured with the ALS and the height obtained from the image-based point clouds at 95% confidence level.

4.3.2. Comparison of tree crown surface from 3D Image-based matching method and Airborne LiDAR

The tree crown surface from two datasets was compared. Table 10 shows the difference in square meters and percentage.

Table 10 the results of comparing tree crown surface from 3D Image-based matching method and airborne LiDAR

Minimum Difference in Square Meters	Maximum Difference in Square Meters	Average Difference in Square Meters	Minimum Difference in %	Maximum Difference in %	Average Difference in %
0.35	1453.26	258.52	0.17	74.79	28.88

The RMSE value is 429.8 square meters and the NRMSE value is 0.551 or 55.1%

The result of the linear regression is shown in Figure 22 and the regression statistics output in Table 11

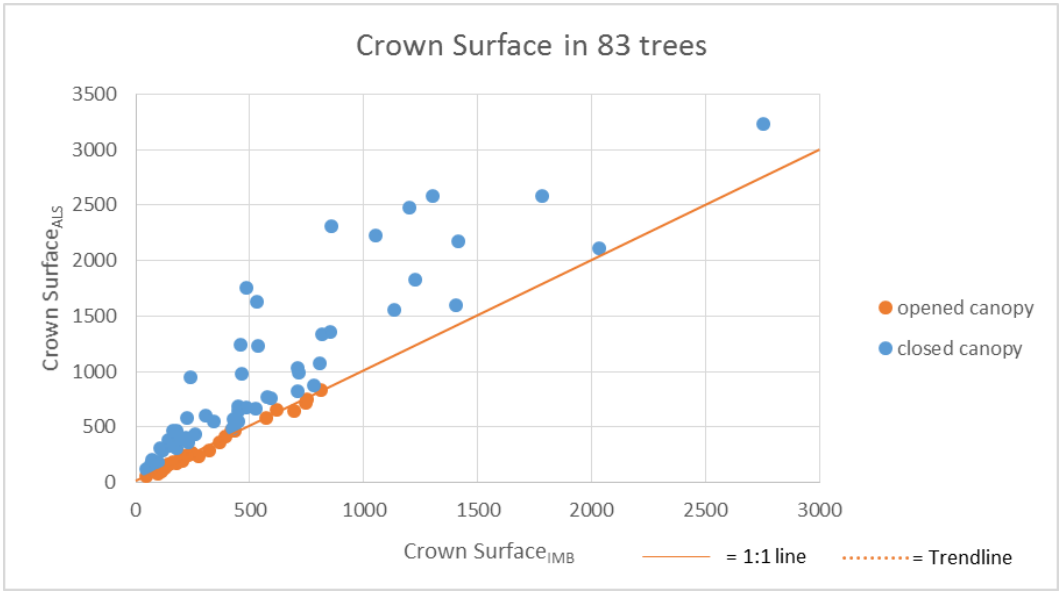

Figure 22 linear regression model of tree crown surface from 3D Image-based point clouds and Airborne LiDAR with trend line and 1:1 line

Table 11 summary of regression statistics output for tree crown surface comparison

Regression Statistics output	
R squared	0.79
Adjust R Squared	0.78
Standard Error	319.28
df	81
F-statistic	308.59
p-value	2.34e-29

The equation obtained from the linear regression is:

Equation 5 tree crown surface equation from regression model

$$Crown\ Surface_{ALS} = (1.3068 \times Crown\ Surface_{IMB}) + 92.427$$

Where, Crown $Surface_{IMB}$ = the value of crown surface area from Image-based point clouds
And Crown $Surface_{ALS}$ = the value of crown surface area from Airborne LiDAR
All unit is in square meter.

The hypothesis to be tested for this research question is:
H_0: The trees crown surface derived from Image-based point clouds is not significantly different from the trees crown surface from airborne LiDAR

Only in the case of solitary trees and trees in a part of the forest with an opened canopy, the null hypothesis cannot be rejected, which means there is no significant difference between the tree crown surface derived from Image-based matching method and tree crown surface measured with the ALS at 95% confidence level.

4.3.3. Assessment of 3D point clouds derived from 3D Image-based matching method and Airborne LiDAR by point-to-point method

In order to assess the matching accuracy of point clouds, the minimum distance of two sets of point clouds, viz. PC_{ALS} and PC_{IMB} was compared. The minimum distance is 0 (perfect match) while the maximum distance is 6.069 meters. The RMSE value for the average distance between two datasets is 0.51 meter while the NRMSE couldn't be calculated because the software were able to give only summarized results. All summarized result of each tree are in appendix IV.

Table 12 summarized results of point-to-point method from Cloudcompare software

Minimum Distance in Meters	Maximum Distance in Meters	Average Distance in Meters	Minimum Sigma (Standard Deviation)	Maximum Sigma (Standard Deviation)	Maximum Relative Error
0	6.06	0.49	0.12	0.70	0.19

The results showed considerable differences between individual trees. Figure 23 shows the histogram of tree number 74. The distances are divided in 8 classes. Tree 74 has 1393 point pairs

in total and most of them (1300) fall in the first distance class (2 – 7 cm) and there are two outliers of 2 and 5 meters distance.

In Figure 24 the histogram of tree number 50 is presented. In this figure the distance between point pairs show a wide spread with the highest frequency in distance class number 3 (51 – 73 centimetres) and the largest distance is 1.81 meters. In this case these differences were cause by the incompleteness of the image-based point cloud (PC_{IMB}), which captured approximately half of the tree because the lack of ground information.

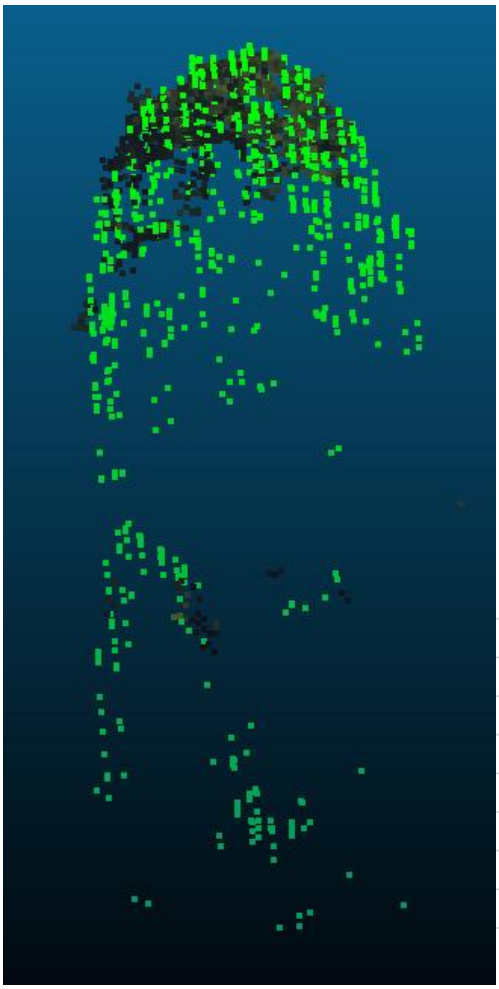

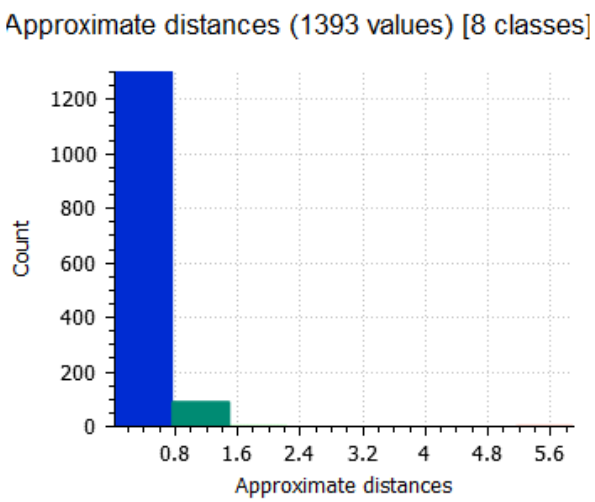

Class	Value	Class start	Class end
1	1300	0.027753334	0.760946675
2	91	0.760946675	1.494140015
3	1	1.494140015	2.227333355
4	0	2.227333355	2.960526695
5	0	2.960526695	3.693720036
6	0	3.693720036	4.426913376
7	0	4.426913376	5.160106716
8	1	5.160106716	5.893300056

Figure 23 tree number 74 in point clouds (Dark colour is PC_{IMB} and green colour is PC_{ALS}), Distance count in histogram (upper right) and distance count in detailed (lower right)

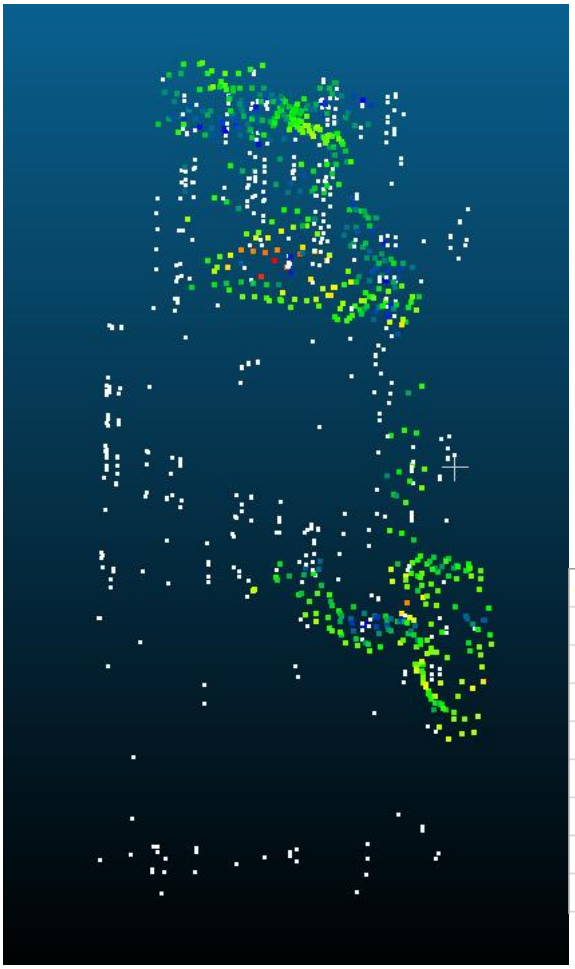

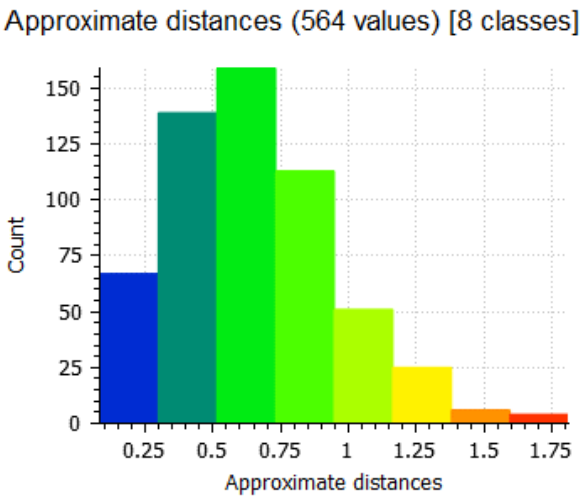

Class	Value	Class start	Class end
1	67	0.082406797	0.2986424
2	139	0.2986424	0.514878003
3	159	0.514878003	0.731113606
4	113	0.731113606	0.947349209
5	51	0.947349209	1.163584813
6	25	1.163584813	1.379820416
7	6	1.379820416	1.596056019
8	4	1.596056019	1.812291622

Figure 24 tree number 50 in point clouds (Colourful point represents PC_{IMB} and white colour is PC_{ALS}), Distance count in histogram (upper right) and distance count in detailed (lower right). The colour of the points related to the colour in histogram.

4.3.4. Comparison of crown height information from 3D Image-based method and Airborne LiDAR

Similar to tree height, the tree crown height from both dataset has been compared for all trees. The summary statistics below described the differences in meters and percentage respectively (see Table 13).

Table 13 the results of comparing tree crown height from 3D Image-based point clouds and airborne LiDAR

Minimum Difference in Meters	Maximum Difference in Meters	Average Difference in Meters	Minimum Difference in %	Maximum Difference in %	Average Difference in %
0	7.05	1.05	0	75.14	11.04

The RMSE value between two datasets for tree crown height is 1.78 meters and the NRMSE value is 0.172 or 17.2%

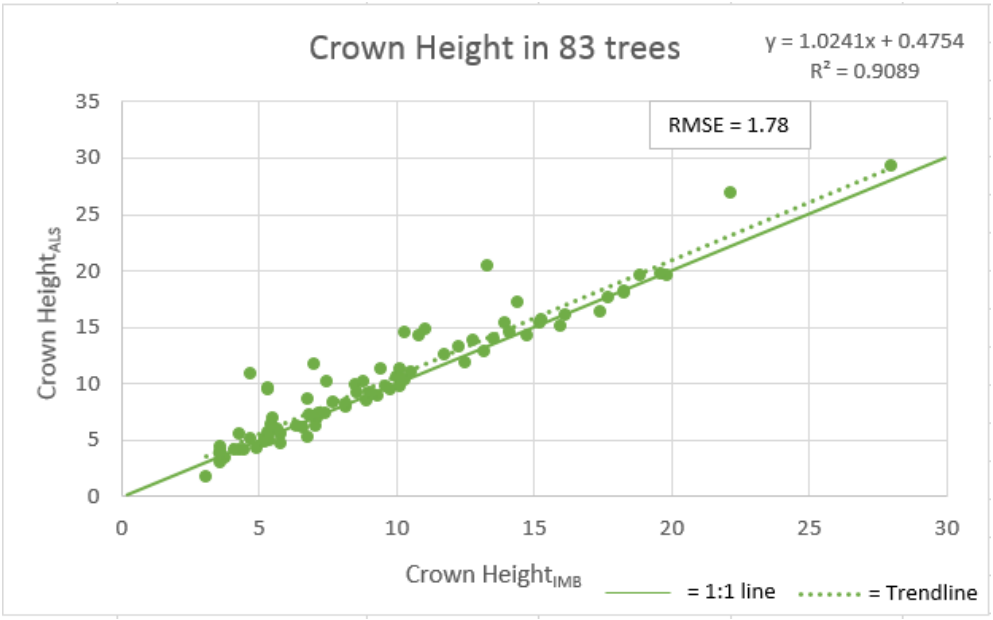

Figure 25 linear regression model of tree crown height from 3D Image-based point clouds and Airborne LiDAR with trend line and 1:1 line

Table 14 summary of regression statistics output for tree crown height comparison

Regression Statistics output	
R squared	0.90
Adjust R Squared	0.90
Standard Error	1.65
df	81
F-statistic	808.39
p-value	6.63e-44

The equation obtained from the linear regression is:

Equation 6 tree crown height equation from regression model

$$Crown\ Height_{ALS} = (1.0241 \times Crown\ Height_{IMB}) + 0.4754$$

Where, $Height_{IMB}$ = Height value from Image-based point clouds
And $Height_{ALS}$ = Height value from Airborne LiDAR; all unit is in meter.

The hypothesis to be tested for this research question is:
H_0: The trees crown height derived from Image-based point clouds is not significantly different from the trees crown height from airborne LiDAR.

Based on the result of the linear regression, the null hypothesis cannot be rejected, which means there is no significant difference between the tree crown height derived from Image-based matching method and tree crown height measured with the ALS at 95% confidence level.

Unlike the results of the tree height comparison, the deviations are smaller and the points are more evenly distributed around the regression line with an NRMSE of 17% instead of 49% in case of tree height. Since this parameter concerns the upper part of the tree and do not need height information from the forest floor, the point clouds are and are expected to be more similar.

5. DISCUSSION

5.1. Discussion for Data Pre-Processing stage

The back-engineering of orthoimage map

The fact that the coordinates of the principal points were missing in the aerial photographs hampered the process, since this information is indispensable for the point cloud generation process. In order to overcome this obstacle, back-engineering of orthoimage map had to be developed, where the georeferenced and geocoded orthophoto had to be used to reconstruct the coordinates of the central points of the original aerial photographs. This process of back-engineering generally leads to an additional spatial inaccuracy (see also the section on bundle block adjustment in this chapter) which in return negatively influences the quality of point clouds. However, the process of point cloud matching (see section 4.2 Data processing; Registration) have probably corrected this error to a certain extent. In the scope of this research this error could not be quantified.

Apart from the missing coordinates of the principal points, the alignment of the flight lines of the aerial photographs also posed a problem, particularly in the Western part of the study area (see Figure 15). Due to the fact that the flight lines were not straight and differed in spacing, the overlap and side lap of the aerial photographs was reduced up to the level that it was insufficient to be used for point cloud extraction. One part of the study around main office of AFHR had no coverage at all. The paper of Hollaus (2015) points out that image matching techniques require a large overlap of individual images in order to retrieve 3D information, and an overlap of 60% and 30% side lap of images is usually required (Wallerman et al., 2015), which the aerial photographs in this study has lower overlap and sidelap than the requirement.

Bundle block adjustment & 3D image-based matching

Because of the complexity of the forest, the flight line distortion and reduced image overlaps, only 29 % of the aerial photographs could be used for bundle block adjustment.

The software used in the study to create point clouds is PIX4D, which is used in various studies (eg. Bhandari et al., 2015; Hernández-clemente et al., 2014; Vetrivel et al., 2015). PIX4D is a black-box software, where the underlying algorithm works in the background and the users can only adapt a limited number of settings. Furthermore, adding a number of ground control points (GCPs) with known coordinates is allowed. Adding GCPs helps the aerial photographs to be better georeferenced which can also found in the study of Ota et al. (2015) that used manually identified ground control points within aerial photographs to improve the accuracy. Ground control points were added where the position of the features could be clearly identified, such as road intersection, corners of structures etc. Linder (2009) also claimed that "5 well-distributed points are the minimum whereas the basic rule is the more the better to get a stable over-determination", which in this study, GCPs more than 5 points were used as full control points (control X, Y and Z).

The PC_{IMB} was prepared from raster data by extracting 3D information from stereo image pairs. Extracting 3D point information from raster stereo image pairs inevitably creates a positional error and the back-engineering process creates another cumulative positional error.

Thus, the quality of the point clouds can be affected by error propagation from these processes. Although quantifying this error was outside of the scope of this research, for future studies it could be recommended that these errors are quantified.

Next to the positional error introduced by the back-engineering process, camera angle and viewing point, depending on the overlap and sidelap, a tree can be present in more than two aerial photographs with differing parallax values and shadow effects, are another source of positional errors in the point cloud generation.

5.2. Discussion for Data Processing stage

Registration (Align) and Segmentation (1)

The first issue of point cloud registration is the homogeneity of forest. The algorithm for doing an automatic registration, like ICP, cannot detect the similarity between two sets of point clouds under these conditions. Therefore the point pairs picking algorithm was the best solution in the primitive registration because the manual selection helped the program to identify easier the correspondence points. And if the datasets are quite different (whether in point characteristics or point density), it is difficult to detect automatically the same points compared to initially help the program to define the same points.

5.3. Discussion for Data Analysis stage

5.3.1. Comparison of tree height from 3D Image-based point clouds and Airborne LiDAR

Out the 83 trees selected for analysis, in 35 trees the difference between $Height_{IMB}$ and $Height_{ALS}$ is more than 20%. As is explained in section 4.3.1, this can be attributed to the forest characteristics. This difference in height measurements is caused by the fact that PC_{IMB} picks up insufficient points from the forest floor in situations with a closed canopy to be able to generate a reliable height data in comparison with PC_{ALS}. These findings concur with the work of Ota et al., 2015. Their paper shows that DTM derived from ALS has a higher accuracy than a DTM derived from the image matching methods. This also conforms to Hollaus, 2015 that ALS gives excellent data for the vertical structure because the laser beams are able to penetrate through small gaps of the canopy down to the forest ground. In the case of tree height, image-based point cloud extraction as alternative for airborne LiDAR is very questionable in situations where it concerns a forest with a closed canopy and when data from the forest floor are required.

5.3.2. Comparison of tree crown surface from 3D Image-based point clouds and Airborne LiDAR

Although the correlation between two dataset is quite good with an r^2 of 0.79 (see Table 11), the variation in crown surface differences is quite high. In 45 out of the 83 trees (54%) the difference in crown surface between aerial images compared to airborne LiDAR data exceeds 20% (see appendix III).

Furthermore, the difference between the tree crown surface from the Airborne LiDAR and from the 3D Image-based point clouds can be clearly seen (see Figure 22). From the scatter plot in figure 23 it becomes clear that the points all lie above the 1:1 line. This means that crown surface derived from PC_{IMB} is systematically lower than PC_{ALS}. Like with the height comparison, this is due to the fact that ALS can penetrate through the forest canopy and provide information about the forest floor, and IMB cannot provide information about lower segments of the tree that are not seen on the aerial images, particularly in the dense canopies.

5.3.3. Assessment of 3D point clouds segmented from 3D Image-based matching method and Airborne LiDAR by point-to-point method

Although the closest distance between point pairs signified the good quality of point clouds, but the high maximum distance value does not indicate that the point pairs are of bad quality. The high value may cause by the outlier data. As seen in 4.3.3 examples, the table in Figure 23 shows that there are two outliers which are in very far distance but the other points from aerial photos performed very close to ALS data. This shows the similarity in terms of correspondence point clouds.

As can be seen in Figure 18 and Figure 24, the point the PC_{ALS} images show horizontal and vertical striping. This effect is caused by the point density of the LiDAR and way images are recorded. During the flight the ALS releases a LiDAR beam at regular intervals. Because the airplane is moving, the beams (appearing as dots in the image) will be aligned along the flight line (see Figure 18) and vertical striping (see Figure 24). This effect does not show up on the PC_{IMB} (see Figure 24), because the algorithm used for point cloud extraction selects points in a more random way. This striping will have an effect on the point to point comparison in the sense that it will increase the distance between a point pair.

5.3.4. Comparison of crown height information from 3D Image-based point clouds and Airborne LiDAR

The crown height information yielded the best result in comparison to the other parameters in this study. This is due to the fact that it only involves the higher part of the canopy and no information of the forest floor is required, With an R^2 of 0.9, an NRMSE of 17% and the fact that the regression line and the 1: 1 line almost coincide it becomes clear that both point clouds are very comparable. This means that for assessment of crown biomass (see Figure 26) PC_{IMB} is an alternative for PC_{ALS}.

For the reason that the crown height result from 3D image-based matching can be counted as comparable as the result from airborne LiDAR, the study of crown biomass itself can be conducted in practicable way. See Figure 26 below for the illustrations of biomass components.

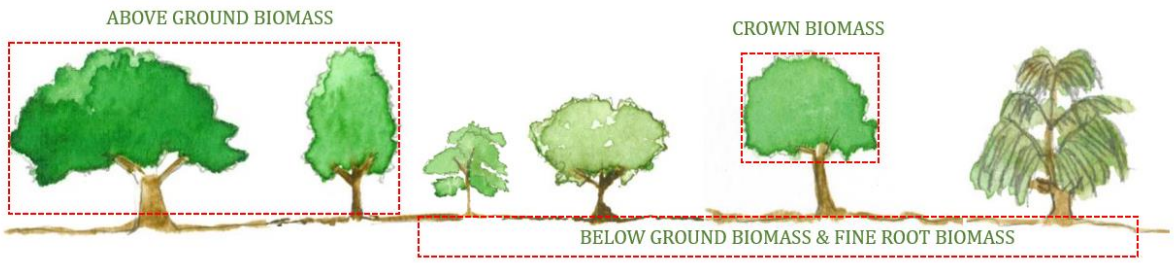

Figure 26 biomass components above and below ground, adapted from (Popescu & Hauglin, 2014)

6. CONCLUSION

The main aim of this study was to investigate if point clouds extracted from stereo aerial photographs (PC_{IMB}) can be used as an alternative for point clouds obtained from Airborne LiDAR Systems (PC_{ALS}) for the assessment of forest parameters (tree height, crown surface, and crown height), using the ALS data as reference. For this purpose three hypotheses were formulated (see secion1.8)

Based on the results of this study none of these null hypotheses could be rejected, which means that there is no significant difference between forest parameters height, crown surface, extracted from PC_{IMB} and PC_{ALS} (see section 4.3)

The best results were obtained for crown height (NRMSE is 17.2%, R^2 is 0.91 and p value is 6.63e-44 at 95% confidence level).

Although the crown surface comparison yields better results than tree height in terms of percentage of variation explained by the model (R^2 is 0.79 and 0.54 respectively), the NRMSE (55% and 48% respectively) and distribution of the points in relation to the 1:1 line (see figure 21 and 22) is similar.

This study shows that height and crown surface extracted from PC_{IMB} only yields good results when compared to height and crown surface extracted from PC_{ALS}, if in the process of image-based point cloud extraction enough information is obtained from the forest floor, a prerequisite which is only met in the case of solitary or more or less free standing tree. The results in dense forest situations with a closed canopy the results are not reliable (see section 4.3)

Summarizing the results of this study shows that image-based point clouds can replace LiDAR point clouds for the assessment of Crown Height. Only in those situations where enough points lying on the forest floor, viz. solitary or more or less free standing trees, can be extracted from the aerial photographs, Image-based point clouds can replace LiDAR based point clouds.

LIST OF REFERENCES

Aalde, H., Gonsalez, P., Gytarsky, M., Krug, T., Kurz, W. A., Lasco, R. D., … Verchot, L. (2006). Chapter2: Generic Methodologies Applicable to Multiple Land-use Categories. *IPCC Guidelines for National Greenhouse Gas Inventories*, 1–59, Retrieved from http://www.ipcc-nggip.iges.or.jp/public/2006gl/vol4.html.

Angelsen, A., & Atmadja, S. (2008). What is this book about? In A. Angelsen (Ed.), *Moving Ahead with REDD Issues , Options and Implications* (pp. 1–10). Bogor: CIFOR. doi:org/10.1002/tqem.3310060102

Ashton, M. S., Tyrrell, M. L., Spalding, D., & Gentry, B. (2012). Managing Forest Carbon in a Changing Climate. Springer.

Besl, P. J., & McKay, N. D. (1992). A Method for Registration of 3-D Shapes. SPIE, 1611, 586–606. doi:org/10.1117/12.57955

Bhandari, B., Oli, U., Pudasaini, U., & Panta, N. (2015). Generation of High Resolution Dsm Using UAV Images. Paper presented at In FIG Working Week 2015: From the Wisdom of the Ages to the Challenges of the Modern World, Sofia. Bulgaria.

Bhattarai, T., Skutsch, M., Midmore, D., & Shrestha, H. (2015). Carbon measurement: An overview of forest carbon estimation methods and the role of GIS and remote sensing techniques for REDD+ implementation. Journal of Forest and Livelihood, 13(1), 71–87.

Chen, Q. (2015). Modeling Aboveground Tree Woody Biomass Using National-Scale Allometric Methods and Airborne Lidar. ISPRS Journal of Photogrammetry and Remote Sensing, 106, 95–106. doi:org/10.1016/j.isprsjprs.2015.05.007

Ciais, P., Sabine, C., Bala, G., Bopp, L., Brovkin, V., Canadell, J., … Thornton, P. (2013). *Carbon and Other Biogeochemical Cycles*. *Climate Change 2013 - The Physical Science Basis*. Retrieved from http://www.ipcc.ch/report/ar5/wg1/

Cihlar, J., Fernandes, R., Fraser, R., Chen, J., Chen, W., Latifovic, R., … Li, Z. (2003). National Scale Forest Information Extraction from Coarse Resolution Satellite Data, Part2: Forest Biophysical Parameters and Carbon. In M. A. Wulder & S. E. Franklin (Eds.), *Remote Sensing of Forest Environments: Concept and Case Studies* (p. 519). Kluwer Academic.

Daniel. (2015a). Cloud-to-Cloud Distance - CloudCompareWiki. Retrieved May 2, 2016, from http://www.cloudcompare.org/doc/wiki/index.php?title=Cloud-to-Cloud_Distance

Daniel. (2015b). ICP - CloudCompareWiki. Retrieved April 30, 2016, from http://www.cloudcompare.org/doc/wiki/index.php?title=ICP

Daniel. (2016). Information for “Align” - CloudCompareWiki. Retrieved May 1, 2016, from http://www.cloudcompare.org/doc/wiki/index.php?title=Align&action=info

Fonstad, M. A., Dietrich, J. T., Courville, B. C., Jensen, J. L., & Carbonneau, P. E. (2013). Topographic structure from motion: A new development in photogrammetric measurement. *Earth Surface Processes and Landforms*, *38*(4), 421–430. doi.org/10.1002/esp.3366

Ginzler, C., & Hobi, M. (2015). Countrywide Stereo-Image Matching for Updating Digital Surface Models in the Framework of the Swiss National Forest Inventory. *Remote Sensing*, *7*(4), 4343–4370. doi:org/10.3390/rs70404343

Hall, R. J. (2003). The Roles of Aerial Photographs in Forestry Remote Sensing Image Analysis. In M. A. Wulder & S. E. Franklin (Eds.), *Remote Sensing of Forest Environments: Concept and Case Studies* (p. 519). Kluwer Academic.

Hernández-clemente, R., Navarro-Cerrillo, R. M., Ramírez, F. J. R., Hornero, A., & Zarco-Tejada, P. J. (2014). A Novel Methodology to Estimate Single-Tree Biophysical Parameters from 3D Digital Imagery Compared to Aerial Laser Scanner Data. *Remote Sensing*, *6*(11), 11627–11648. doi:org/10.3390/rs61111627

Hollaus, M. (2015). 3D Point Clouds for Forestry Applications. *Vermessung&Geoinformation*, 138–150.

IPCC. (2014). *Climate Change 2014 Synthesis Report Summary Chapter for Policymakers*. *Ipcc*. Retrieved from http://www.ipcc.ch/report/ar5/syr/

Ismail, M. H., & Mohamed, K. A. (2008). Interactive 3D Image of Ayer Hitam Forest Reserve from Triangular Irregular Network (TIN) layers by Draping Technique. *Buletin Geospatial Sektor*

Awam, (December). Retrieved from http://www.mygeoportal.gov.my/sites/default/files/Interactive 3D_Dr Hasmadi.pdf
Kato, A., Kajiwara, K., Honda, Y., Watanabe, M., Enoki, T., Yamaguchi, Y., & Kobayashi, T. (2014). Efficient Field Data Collection of Tropical Forest Using Terrestrial Laser Scanner. In IGARSS 2014: Energy and our Changing Planet (pp. 816–819). Quebec: 2014 IEEE Geoscience and Remote Sensing Symposium. doi:org/10.1109/IGARSS.2014.6946549
Katoch, C. (2013). Photogrammetric Applications for 3-D realistic reconstruction of objects using still images. University of Twente, Faculty of Geo-information Science and Earth Observation (ITC). MSc thesis.
Koch, B., Kattenborn, T., Straub, C., & Vauhkonen, J. (2014). Segmentation of Forest to Tree Objects. In M. Maltamo, E. Næsset, & J. Vauhkonen (Eds.), *Forestry Applications of Airborne Laser Scanning Concepts and Case Studies* (pp. 88–112). Springer. doi.org/10.1007/978-94-017-8663-8
Kugler, F., Lee, S., Hajnsek, I., & Papathanassiou, K. P. (2015). Forest Height Estimation by Means of Pol-InSAR Data Inversion : The Role of the Vertical Wavenumber. *IEEE Transactions on Geoscience and Remote Sensing*, *53*(10), 5294–5311.
Lefsky, M. a, Cohen, W. B., Parker, G. G., & Harding, D. J. (2002). Lidar Remote Sensing for Ecosystem Studies, *52*(1), 19–30.
Lepun, P., Faridah, H. I., & Jusoff, K. (2007). Tree Species Distribution in Ayer Hitam Forest Reserve, Selangor, Malaysia. *Proceedings of the 3rd IASMEWSEAS International Conference on Energy Environment Ecosystems and Sustainable Development*, 75–81.
Li, W., Niu, Z., Liang, X., Li, Z., Huang, N., Gao, S., … Muhammad, S. (2015). Geostatistical Modeling Using LiDAR-Derived Prior Knowledge with SPOT-6 data to Estimate Temperate Forest Canopy Cover and Above-Ground Biomass via Stratified Random Sampling. *International Journal of Applied Earth Observations and Geoinformation*, *41*, 88–98. doi:org/10.1016/j.jag.2015.04.020
Liang, X., Wang, Y., Jaakkola, A., Kukko, A., Kaartinen, H., Hyyppä, J., … Liu, J. (2015). Forest Data Collection Using Terrestrial Image-Based Point Clouds From a Handheld Camera Compared to Terrestrial and Personal Laser Scanning. *IEEE Transactions on Geoscience and Remote Sensing*, *53*(9), 5117–5132. http://doi.org/10.1109/TGRS.2015.2417316
Lim, K., Treitz, P., Wulder, M., St-Onge, B., & Flood, M. (2003). LiDAR remote sensing of forest structure. *Progress in Physical Geography*, *27*(1), 88–106. doi:org/10.1191/0309133303pp360ra
Linder, W. (2009). *Digital photogrammetry: A Practical Course* (Third). Heidelberg: Springer-Verlag Berlin Heidelberg. doi:org/10.1007/978-3-540-92725-9
Lubowski, R. N. (2008). What are the costs and potentials of REDD? In A. Angelsen (Ed.), *Moving Ahead with REDD Issues, Options and Implications* (pp. 23–156). Bogor: CIFOR. doi:org/10.1002/tqem.3310060102
Mitchell, H. (2007). Fundamental of Photogrammetry. In J. Fryer, H. Mitchell, & J. Chandler (Eds.), *Application of 3D Measurement from Images* (pp. 9–36). Scotland, UK: Whittles Publishing.
Mursa, P. (2013). Forest Parameter Estimation by Lidar Data Processing. *RevCAD Journal of Geodesy and Cadastre*, *14*, 27–36.
Nuttall, N. (2015). About UNFCCC. Retrieved August 19, 2015, from http://newsroom.unfccc.int/about/
Ota, T., Ogawa, M., Shimizu, K., Kajisa, T., Mizoue, N., Yoshida, S., … Ket, N. (2015). Aboveground biomass estimation using structure from motion approach with aerial photographs in a seasonal tropical forest. *Forests*, *6*(11), 3882–3898. doi:org/10.3390/f6113882
Pan, Y., Birdsey, R. a, Fang, J., Houghton, R., Kauppi, P. E., Kurz, W. a, … Hayes, D. (2011). A Large and Persistent Carbon Sink in the World's Forests. *Science (New York, N.Y.)*, *333*(6045), 988–993. doi:org/10.1126/science.1201609
Paneque-Gálvez, J., McCall, M. K., Napoletano, B. M., Wich, S. a., & Koh, L. P. (2014). Small Drones for Community-Based Forest Monitoring: An Assessment of Their Feasibility and Potential in Tropical Areas. *Forests*, *5*(6), 1481–1507. doi:org/10.3390/f5061481
Pears, N., Yonghuai, L., & Bunting, P. (Eds.). (2012). *3D Imaging, Analysis and Application*. Springer.
PIX4D. (2016a). Menu Process > Processing Options... > 2. Point Cloud and Mesh > Point Cloud –

Support. Retrieved May 1, 2016, from https://support.pix4d.com/hc/en-us/articles/202557799-Menu-Process-Processing-Options-2-Point-Cloud-and-Mesh-Point-Cloud#gsc.tab=0
PIX4D. (2016b). TOOLS - GSD Calculator. Retrieved May 20, 2016, from https://support.pix4d.com/hc/en-us/articles/202560249-TOOLS-GSD-Calculator#gsc.tab=0
Popescu, S. C., & Hauglin, M. (2014). Estimation of Biomass Components by Airborne Laser Scanning. In M. Maltamo, E. Næsset, & J. Vauhkonen (Eds.), Forestry Applications of Airborne Laser Scanning Concepts and Case Studies (pp. 157–172). Springer. doi:org/10.1007/978-94-017-8663-8
Ravindranath, N. H., & Ostwald, M. (2008). Carbon Inventory Methods: Handbook for Greenhouse Gas Inventory, Carbon Mitigation and Roundwood Production Projects. (M. Beniston, Ed.). Springer.
Renslow, M. S. (2012). Manual of Airborne Topographic LiDAR. American Society for Photogrammetry and Remote Sensing.Silva, C. A., Crookston, N. L., Hudak, A. T., & Vierling, L. A. (2015). Package "rLiDAR." Retrieved March 2, 2016, from https://cran.r-project.org/web/packages/rLiDAR/rLiDAR.pdf
St-Onge, B., Audet, F.-A., & Bégin, J. (2015). Characterizing the Height Structure and Composition of a Boreal Forest Using an Individual Tree Crown Approach Applied to Photogrammetric Point Clouds. Forests, 6(11), 3899–3922. doi.org/10.3390/f6113899
Silva, C. A., Crookston, N. L., Hudak, A. T., & Vierling, L. A. (2015). Package "rLiDAR." Retrieved March 2, 2016, from https://cran.r-project.org/web/packages/rLiDAR/rLiDAR.pdf
Vetrivel, A., Gerke, M., Kerle, N., & Vosselman, G. (2015). Identification of damage in buildings based on gaps in 3D point clouds from very high resolution oblique airborne images. ISPRS Journal of Photogrammetry and Remote Sensing, 105, 61–78. doi:org/10.1016/j.isprsjprs.2015.03.016
Vosselman, G., & Maas, H.-G. (2010). Airborne and Terrestrial Laser Scanning. Scotland, UK: Whittles Publishing.
Wallerman, J., Nyström, K., Bohlin, J., Persson, H. J., Soja, M. J., & Fransson, J. E. S. (2015). Estimating Forest Age and Site Productivity Using Time Series of 3D Remote Sensing Data. IEEE, 3321-3324.
White, J., Wulder, M., Vastaranta, M., Coops, N., Pitt, D., & Woods, M. (2013). The Utility of Image-Based Point Clouds for Forest Inventory: A Comparison with Airborne Laser Scanning. Forests, 4(3), 518–536. http://doi.org/10.3390/f4030518Wulder, M., & Franklin, S. E. (2003). Remote Sensing of Forest Environments, Introduction: the Transition from Theory to Information. In *Remote Sensing of Forest Environments: Concept and Case Studies* (p. 519). Kluwer Academic.
Wulder, M., & Franklin, S. E. (2003). Remote Sensing of Forest Environments, Introduction: the Transition from Theory to Information. In Remote Sensing of Forest Environments: Concept and Case Studies (p. 519). Kluwer Academic.
Zhang, C., Zhou, Y., & Qiu, F. (2015). Individual Tree Segmentation from LiDAR Point Clouds for Urban Forest Inventory. *Remote Sensing*, *7*(6), 7892–7913. doi.org/10.3390/rs70607892

APPENDICES

Appendix I: Table showing the height per tree derived from ALS and image-based point clouds (high and optimal density)

Tree number	ALS (m)	High Density (m)	Optimal Density (m)	%Difference High Density	%Difference Optimal Density
1	7.74	8.7	7.71	12.40	0.39
2	17.21	5.57	4.58	67.64	73.39
3	4.34	4.55	4.35	4.84	0.23
4	13.6	5.61	3.84	58.75	71.76
5	17.02	6.09	7.03	64.22	58.70
6	24.74	37.95	37.62	53.40	52.06
7	26.16	14.02	19.25	46.41	26.41
8	7.63	8.42	8.34	10.35	9.31
9	28.31	4.91	16.13	82.66	43.02
10	24.02	11.22	12.12	53.29	49.54
11	16.27	4.38	4.27	73.08	73.76
12	7.52	15.42	8.48	105.05	12.77
13	8.94	8.52	8.37	4.70	6.38
14	6.32	7.86	8.41	24.37	33.07
15	28.45	9.48	7.63	66.68	73.18
Average difference of all trees				48.52%	38.93%
Standard Deviation of all trees				29.70%	27.25%
Average difference of trees in open canopy				26.95%	10.36%
Standard Deviation of trees in open canopy				35.54%	11.11%

(Where; ALS = point clouds derived from ALS;
High Density and Optimal density = point clouds derived from image matching method; Highlighted information for tree number 1, 3, 8, 12-14 are derived from trees in open area; %Difference High Density and Optimal Density = difference in percentage differed from height value of ALS)

From aforementioned table, there were 15 trees randomly selected from a subset in the study area including trees within the closed canopy and trees in the open area. Obviously, tree number 1, 3, 8, and 12-14 are in the open area which, the ground information were available for the image matching method. As those information can be used to measure the height of the trees. While this method were not able to retrieve the real height of the trees in the closed canopy due to the lack of ground information. The lowest point of the trees retrieved from image matching method were used to measure the tree height instead. All differences used ALS height as a base height.

The result of this comparison shows that the height average difference of all 15 trees in high density is 48.52% while the optimal density is 38.93% whereas the height average difference of 6 trees in an open area are 26.95% and 10.36% for high and optimal density respectively.

Appendix II: Tree height information from PC_{ALS} and PC_{IMB}

Tree Number	Height from ALS (m)	Height from Aerial photos (m)	Difference (m)	Difference (absolute value) (m)	Difference in % (ALS as a reference)
1	9.40	10.13	-0.73	0.73	7.78
2	8.45	8.81	-0.36	0.36	4.26
3	19.68	12.80	6.88	6.88	-34.96
4	14.73	7.16	7.57	7.57	-51.39
5	4.46	4.69	-0.23	0.23	5.16
6	28.25	24.29	3.96	3.96	-14.02
7	27.08	18.64	8.44	8.44	-31.17
8	27.36	19.86	7.50	7.50	-27.41
9	12.64	5.48	7.16	7.16	-56.65
10	11.53	11.61	-0.08	0.08	0.69
11	15.19	5.55	9.64	9.64	-63.46
12	21.32	9.43	11.89	11.89	-55.77
13	17.86	4.28	13.58	13.58	-76.04
14	18.43	5.80	12.63	12.63	-68.53
15	15.65	9.89	5.76	5.76	-36.81
16	16.50	3.69	12.81	12.81	-77.64
17	10.64	3.62	7.02	7.02	-65.98
18	21.96	8.52	13.44	13.44	-61.20
19	11.89	14.18	-2.29	2.29	19.26
20	13.54	5.27	8.27	8.27	-61.08
21	24.04	21.53	2.51	2.51	-10.44
22	19.23	4.70	14.53	14.53	-75.56
23	10.21	8.64	1.57	1.57	-15.38
24	6.37	6.72	-0.35	0.35	5.49
25	28.95	13.70	15.25	15.25	-52.68
26	9.16	9.10	0.06	0.06	-0.66
27	23.91	16.30	7.61	7.61	-31.83
28	16.90	15.30	1.60	1.60	-9.48
29	12.45	12.62	-0.17	0.17	1.37
30	7.79	7.70	0.09	0.09	-1.16
31	4.32	4.65	-0.33	0.33	7.64
32	16.72	17.17	-0.45	0.45	2.69
33	6.68	7.20	-0.52	0.52	7.78
34	5.94	6.29	-0.35	0.35	5.89
35	6.81	6.89	-0.08	0.08	1.17
36	4.82	4.96	-0.14	0.14	2.90
37	7.42	7.14	0.28	0.28	-3.77
38	13.91	14.21	-0.30	0.30	2.16
39	7.02	7.20	-0.18	0.18	2.56
40	16.06	16.40	-0.34	0.34	2.12

Tree Number	Height from ALS (m)	Height from Aerial photos (m)	Difference (m)	Difference (absolute value) (m)	Difference in % (ALS as a reference)
41	13.33	13.10	0.23	0.23	-1.73
42	10.98	11.37	-0.39	0.39	3.55
43	15.94	12.35	3.59	3.59	-22.52
44	8.08	6.87	1.21	1.21	-14.98
45	12.74	12.54	0.20	0.20	-1.57
46	14.60	14.56	0.04	0.04	-0.27
47	12.46	12.49	-0.03	0.03	0.24
48	13.51	8.29	5.22	5.22	-38.64
49	15.21	6.94	8.27	8.27	-54.37
50	17.13	14.13	3.00	3.00	-17.51
51	45.03	40.83	4.20	4.20	-9.33
52	42.31	12.56	29.75	29.75	-70.31
53	37.27	10.28	26.99	26.99	-72.42
54	38.64	15.97	22.67	22.67	-58.67
55	32.41	14.42	17.99	17.99	-55.51
56	46.25	28.02	18.23	18.23	-39.42
57	32.12	30.49	1.63	1.63	-5.07
58	37.22	37.06	0.16	0.16	-0.43
59	33.05	10.56	22.49	22.49	-68.05
60	48.72	22.16	26.56	26.56	-54.52
61	28.90	28.76	0.14	0.14	-0.48
62	13.06	6.79	6.27	6.27	-48.01
63	15.13	15.58	-0.45	0.45	2.97
64	5.62	5.78	-0.16	0.16	2.85
65	21.73	21.76	-0.03	0.03	0.14
66	23.29	16.18	7.11	7.11	-30.53
67	37.87	35.50	2.37	2.37	-6.26
68	41.60	20.36	21.24	21.24	-51.06
69	30.08	30.12	-0.04	0.04	0.13
70	36.45	35.13	1.32	1.32	-3.62
71	30.05	11.05	19.00	19.00	-63.23
72	23.20	22.50	0.70	0.70	-3.02
73	33.59	30.87	2.72	2.72	-8.10
74	34.49	23.43	11.06	11.06	-32.07
75	11.56	4.11	7.45	7.45	-64.45
76	7.73	8.29	-0.56	0.56	7.24
77	17.19	16.85	0.34	0.34	-1.98
78	36.88	21.77	15.11	15.11	-40.97
79	24.62	13.94	10.68	10.68	-43.38
80	7.10	7.15	-0.05	0.05	0.70
81	13.54	13.43	0.11	0.11	-0.81
82	25.82	26.21	-0.39	0.39	1.51
83	18.44	19.10	-0.66	0.66	3.58

Appendix III: Tree crown surface information from PC_{ALS} and PC_{IMB}

Tree Number	Crown Surface from ALS (m^2)	Crown Surface from Aerial photos (m^2)	Difference (m^2)	Difference (absolute value) (m^2)	Difference in % (ALS as a reference)
1	187.81	164.52	23.29	87.60	-12.40
2	128.47	126.36	2.11	98.35	-1.65
3	575.21	428.19	147.02	74.44	-25.56
4	307.94	176.09	131.84	57.18	-42.82
5	79.20	94.46	-15.26	119.26	19.26
6	875.46	779.03	96.43	88.98	-11.02
7	597.83	306.20	291.63	51.22	-48.78
8	681.78	451.13	230.65	66.17	-33.83
9	334.01	152.10	181.91	45.54	-54.46
10	648.87	696.68	-47.81	107.37	7.37
11	399.34	194.48	204.86	48.70	-51.30
12	408.39	220.11	188.28	53.90	-46.10
13	313.03	106.95	206.07	34.17	-65.83
14	387.56	144.81	242.75	37.37	-62.63
15	362.82	230.01	132.81	63.40	-36.60
16	165.72	65.64	100.07	39.61	-60.39
17	124.28	43.51	80.77	35.01	-64.99
18	579.44	223.41	356.03	38.56	-61.44
19	462.85	435.12	27.73	94.01	-5.99
20	290.58	116.25	174.32	40.01	-59.99
21	523.68	433.72	89.96	82.82	-17.18
22	467.15	163.37	303.78	34.97	-65.03
23	241.63	198.68	42.95	82.22	-17.78
24	167.11	144.61	22.50	86.54	-13.46
25	978.81	464.13	514.68	47.42	-52.58
26	358.87	367.75	-8.88	102.47	2.47
27	679.03	482.71	196.33	71.09	-28.91
28	660.86	525.48	135.38	79.51	-20.49
29	653.60	619.28	34.32	94.75	-5.25
30	253.69	248.10	5.59	97.80	-2.20
31	55.25	44.30	10.95	80.17	-19.83
32	766.57	577.54	189.03	75.34	-24.66
33	159.52	144.80	14.73	90.77	-9.23
34	201.67	202.03	-0.36	100.18	0.18
35	286.30	319.28	-32.98	111.52	11.52
36	174.54	177.09	-2.55	101.46	1.46
37	101.98	111.51	-9.53	109.34	9.34
38	721.90	744.41	-22.52	103.12	3.12
39	245.31	229.63	15.68	93.61	-6.39
40	757.75	594.05	163.70	78.40	-21.60
41	490.60	425.75	64.85	86.78	-13.22

Tree Number	Crown Surface from ALS (m^2)	Crown Surface from Aerial photos (m^2)	Difference (m^2)	Difference (absolute value) (m^2)	Difference in % (ALS as a reference)
42	410.21	391.25	18.96	95.38	-4.62
43	644.95	449.24	195.71	69.66	-30.34
44	220.15	203.65	16.51	92.50	-7.50
45	272.36	245.80	26.56	90.25	-9.75
46	548.96	450.43	98.53	82.05	-17.95
47	467.81	420.80	47.01	89.95	-10.05
48	987.23	715.84	271.38	72.51	-27.49
49	461.05	179.86	281.18	39.01	-60.99
50	435.39	260.42	174.97	59.81	-40.19
51	2581.12	1785.43	795.70	69.17	-30.83
52	1759.49	487.24	1272.25	27.69	-72.31
53	1629.32	528.65	1100.68	32.45	-67.55
54	1245.12	460.04	785.09	36.95	-63.05
55	1226.97	538.00	688.97	43.85	-56.15
56	2580.03	1304.51	1275.52	50.56	-49.44
57	1070.64	809.17	261.48	75.58	-24.42
58	1557.21	1136.43	420.78	72.98	-27.02
59	948.61	239.14	709.47	25.21	-74.79
60	2310.81	857.54	1453.27	37.11	-62.89
61	1361.23	853.44	507.79	62.70	-37.30
62	181.44	94.72	86.72	52.20	-47.80
63	580.86	572.26	8.60	98.52	-1.48
64	190.43	204.40	-13.97	107.33	7.33
65	2115.59	2032.13	83.46	96.05	-3.95
66	1031.47	709.95	321.52	68.83	-31.17
67	1594.53	1403.57	190.96	88.02	-11.98
68	2478.65	1199.37	1279.28	48.39	-51.61
69	836.31	812.88	23.43	97.20	-2.80
70	2170.52	1417.27	753.24	65.30	-34.70
71	2229.09	1051.89	1177.21	47.19	-52.81
72	824.98	711.18	113.79	86.21	-13.79
73	3228.11	2752.68	475.43	85.27	-14.73
74	1333.94	819.21	514.73	61.41	-38.59
75	200.00	69.82	130.18	34.91	-65.09
76	240.09	276.24	-36.15	115.06	15.06
77	754.11	750.07	4.03	99.47	-0.53
78	1828.83	1223.81	605.02	66.92	-33.08
79	553.85	342.49	211.36	61.84	-38.16
80	173.10	184.64	-11.54	106.67	6.67
81	741.35	579.54	161.81	78.17	-21.83
82	1088.94	1068.76	20.18	98.15	-1.85
83	719.31	648.76	70.55	90.19	-9.81

Appendix IV: Distance between point-to-point from PC_{ALS} and PC_{IMB}

Tree Number	Min Distance(m)	Max Distance (m)	Average distance (m)	Sigma (m)	Max Error
1	0.00	1.54	0.52	0.25	0.04
2	0.10	2.22	0.63	0.40	0.03
3	0.00	2.58	0.48	0.30	0.08
4	0.00	1.27	0.35	0.21	0.06
5	0.05	2.92	0.90	0.53	0.02
6	0.00	3.32	0.59	0.48	0.11
7	0.00	2.13	0.62	0.40	0.11
8	0.00	2.16	0.54	0.36	0.11
9	0.00	1.29	0.30	0.17	0.05
10	0.00	2.86	0.55	0.36	0.06
11	0.00	1.21	0.32	0.16	0.06
12	0.00	2.52	0.52	0.33	0.09
13	0.00	1.45	0.54	0.25	0.07
14	0.00	1.68	0.37	0.24	0.07
15	0.00	2.67	0.67	0.45	0.06
16	0.00	0.98	0.26	0.13	0.07
17	0.08	0.77	0.33	0.13	0.04
18	0.00	1.12	0.44	0.20	0.09
19	0.00	2.35	0.69	0.39	0.06
20	0.00	1.39	0.44	0.21	0.05
21	0.00	3.38	0.58	0.39	0.09
22	0.00	1.19	0.35	0.20	0.08
23	0.00	1.45	0.35	0.19	0.04
24	0.00	2.03	0.40	0.31	0.03
25	0.00	2.30	0.46	0.33	0.12
26	0.00	2.03	0.65	0.37	0.05
27	0.00	2.68	0.51	0.33	0.10
28	0.00	2.12	0.38	0.22	0.07
29	0.00	2.15	0.44	0.22	0.06
30	0.00	1.18	0.36	0.19	0.04
31	0.07	0.91	0.40	0.18	0.02
32	0.00	2.37	0.47	0.30	0.07
33	0.06	1.36	0.45	0.23	0.03
34	0.00	1.66	0.43	0.26	0.04
35	0.00	1.98	0.50	0.32	0.05
36	0.00	1.38	0.46	0.24	0.04
37	0.00	2.05	0.55	0.37	0.03
38	0.00	2.86	0.68	0.40	0.06
39	0.00	1.52	0.43	0.20	0.04
40	0.00	2.64	0.59	0.34	0.07
41	0.00	2.07	0.49	0.26	0.05

Tree Number	Min Distance(m)	Max Distance (m)	Average distance (m)	Sigma (m)	Max Error
42	0.00	2.28	0.45	0.25	0.05
43	0.00	2.70	0.66	0.41	0.06
44	0.00	1.50	0.39	0.22	0.04
45	0.00	2.04	0.59	0.34	0.05
46	0.00	2.54	0.40	0.21	0.06
47	0.00	2.73	0.53	0.43	0.05
48	0.00	1.97	0.44	0.26	0.08
49	0.00	1.80	0.45	0.23	0.06
50	0.00	1.83	0.64	0.31	0.07
51	0.00	3.59	0.55	0.39	0.18
52	0.00	2.76	0.54	0.37	0.17
53	0.00	3.22	0.41	0.29	0.15
54	0.00	1.69	0.39	0.27	0.15
55	0.00	2.65	0.47	0.33	0.13
56	0.00	4.18	0.62	0.49	0.18
57	0.00	4.43	0.92	0.70	0.13
58	0.00	3.66	0.57	0.52	0.15
59	0.00	1.57	0.51	0.27	0.13
60	0.00	3.05	0.59	0.43	0.19
61	0.00	1.80	0.40	0.25	0.11
62	0.00	1.79	0.48	0.26	0.05
63	0.00	2.62	0.53	0.32	0.06
64	0.00	2.60	0.62	0.52	0.04
65	0.00	2.80	0.68	0.38	0.11
66	0.00	2.03	0.41	0.27	0.09
67	0.00	6.07	0.60	0.51	0.15
68	0.00	2.95	0.48	0.39	0.16
69	0.00	5.57	0.57	0.48	0.12
70	0.00	3.19	0.45	0.35	0.14
71	0.00	2.08	0.28	0.24	0.12
72	0.00	1.87	0.46	0.30	0.09
73	0.00	2.70	0.41	0.33	0.13
74	0.00	5.79	0.38	0.27	0.14
75	0.00	1.00	0.30	0.16	0.05
76	0.00	2.45	0.62	0.46	0.04
77	0.00	3.09	0.43	0.30	0.07
78	0.00	2.68	0.51	0.39	0.15
79	0.00	2.26	0.64	0.38	0.10
80	0.10	2.35	0.51	0.35	0.03
81	0.00	2.12	0.40	0.26	0.06
82	0.00	2.60	0.53	0.37	0.10
83	0.00	2.12	0.44	0.30	0.08

Appendix V: Tree crown height information from PC_{ALS} and PC_{IMB}

Tree Number	Crown Height from ALS(m)	Crown Height from Aerial photos (m)	Difference (m)	Difference (absolute value) (m)	Difference in % (ALS as a reference)
1	7.93	8.15	-0.22	0.22	102.77
2	6.29	7.06	-0.77	0.77	112.24
3	13.84	12.80	1.04	1.04	92.49
4	7.24	6.86	0.38	0.38	94.75
5	1.77	3.10	-1.33	1.33	175.14
6	10.17	7.47	2.70	2.70	73.45
7	18.16	18.30	-0.14	0.14	100.77
8	19.62	19.86	-0.24	0.24	101.22
9	6.37	5.44	0.93	0.93	85.40
10	9.83	9.59	0.24	0.24	97.56
11	6.92	5.51	1.41	1.41	79.62
12	11.36	9.41	1.95	1.95	82.83
13	5.57	4.28	1.29	1.29	76.84
14	5.15	5.21	-0.06	0.06	101.17
15	9.49	9.81	-0.32	0.32	103.37
16	3.41	3.75	-0.34	0.34	109.97
17	4.04	3.62	0.42	0.42	89.60
18	9.91	8.52	1.39	1.39	85.97
19	9.24	9.01	0.23	0.23	97.51
20	9.45	5.31	4.14	4.14	56.19
21	11.71	7.01	4.70	4.70	59.86
22	10.84	4.70	6.14	6.14	43.36
23	4.38	3.60	0.78	0.78	82.19
24	3.44	3.74	-0.30	0.30	108.72
25	12.85	13.22	-0.37	0.37	102.88
26	7.02	7.11	-0.09	0.09	101.28
27	9.78	10.12	-0.34	0.34	103.48
28	9.21	8.56	0.65	0.65	92.94
29	10.56	9.99	0.57	0.57	94.60
30	5.09	4.71	0.38	0.38	92.53
31	2.96	3.61	-0.65	0.65	121.96
32	13.27	12.27	1.00	1.00	92.46
33	4.35	4.94	-0.59	0.59	113.56
34	4.98	5.39	-0.41	0.41	108.23
35	4.67	5.77	-1.10	1.10	123.55
36	4.15	4.27	-0.12	0.12	102.89
37	5.74	5.36	0.38	0.38	93.38
38	8.97	9.30	-0.33	0.33	103.68
39	5.59	5.77	-0.18	0.18	103.22
40	8.47	8.90	-0.43	0.43	105.08
41	10.47	10.13	0.34	0.34	96.75

Tree Number	Crown Height from ALS(m)	Crown Height from Aerial photos (m)	Difference (m)	Difference (absolute value) (m)	Difference in % (ALS as a reference)
42	7.31	7.16	0.15	0.15	97.95
43	10.32	10.32	0.00	0.00	100.00
44	3.71	3.60	0.11	0.11	97.04
45	6.26	6.40	-0.14	0.14	102.24
46	8.22	8.17	0.05	0.05	99.39
47	7.42	7.44	-0.02	0.02	100.27
48	8.37	7.70	0.67	0.67	92.00
49	7.08	6.94	0.14	0.14	98.02
50	5.93	5.66	0.27	0.27	95.45
51	19.54	18.89	0.65	0.65	96.67
52	20.39	13.34	7.05	7.05	65.42
53	14.50	10.28	4.22	4.22	70.90
54	15.16	15.97	-0.81	0.81	105.34
55	17.24	14.42	2.82	2.82	83.64
56	29.28	28.02	1.26	1.26	95.70
57	9.12	9.13	-0.01	0.01	100.11
58	12.60	11.76	0.84	0.84	93.33
59	11.00	10.56	0.44	0.44	96.00
60	26.83	22.16	4.67	4.67	82.59
61	9.63	5.32	4.31	4.31	55.24
62	8.60	6.79	1.81	1.81	78.95
63	6.04	6.63	-0.59	0.59	109.77
64	4.21	4.45	-0.24	0.24	105.70
65	17.65	17.68	-0.03	0.03	100.17
66	13.91	13.52	0.39	0.39	97.20
67	15.38	15.23	0.15	0.15	99.02
68	19.70	19.60	0.10	0.10	99.49
69	10.20	8.80	1.40	1.40	86.27
70	15.67	15.30	0.37	0.37	97.64
71	14.79	11.05	3.74	3.74	74.71
72	14.25	14.76	-0.51	0.51	103.58
73	18.00	18.29	-0.29	0.29	101.61
74	14.24	10.80	3.44	3.44	75.84
75	4.14	4.11	0.03	0.03	99.28
76	5.28	6.76	-1.48	1.48	128.03
77	11.25	10.11	1.14	1.14	89.87
78	14.55	14.14	0.41	0.41	97.18
79	15.43	13.94	1.49	1.49	90.34
80	4.79	5.21	-0.42	0.42	108.77
81	11.89	12.53	-0.64	0.64	105.38
82	16.13	16.12	0.01	0.01	99.94
83	16.39	17.40	-1.01	1.01	106.16

Appendix VI: Histogram from point-to-point distance method between ALS and IMB (by using ALS as a reference)

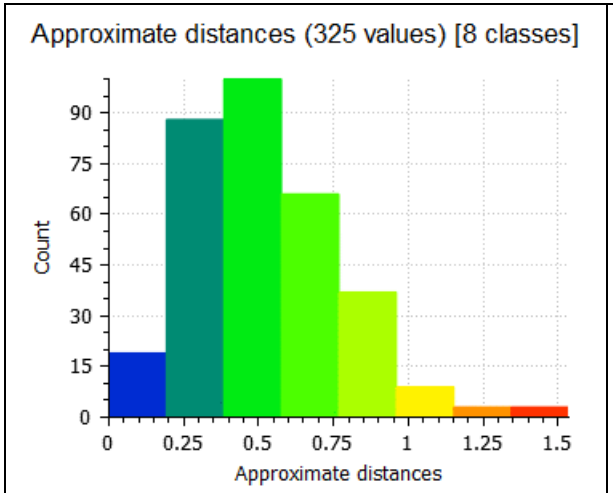

Tree1

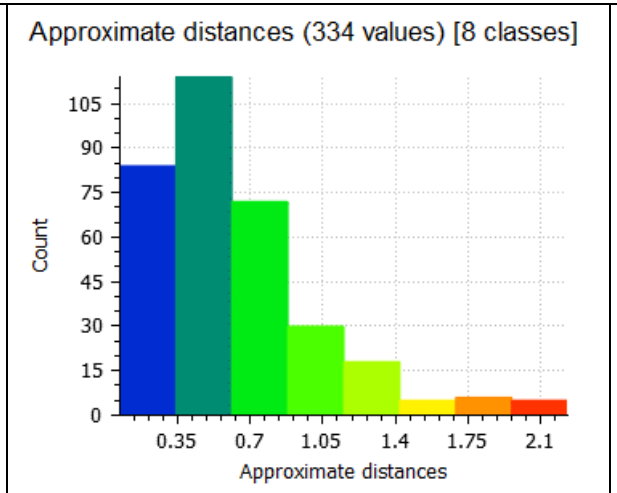

Tree2

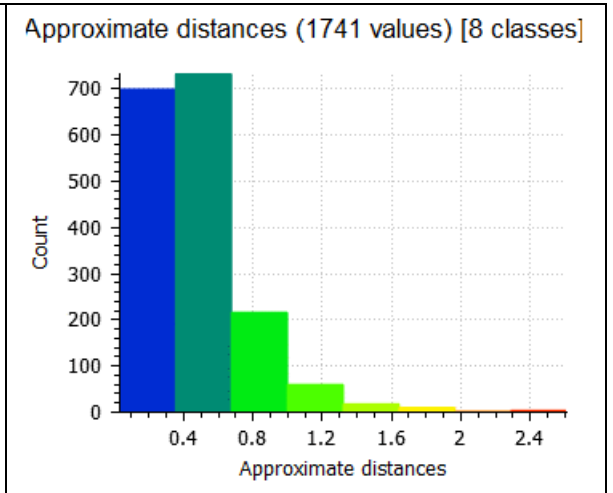

Tree3

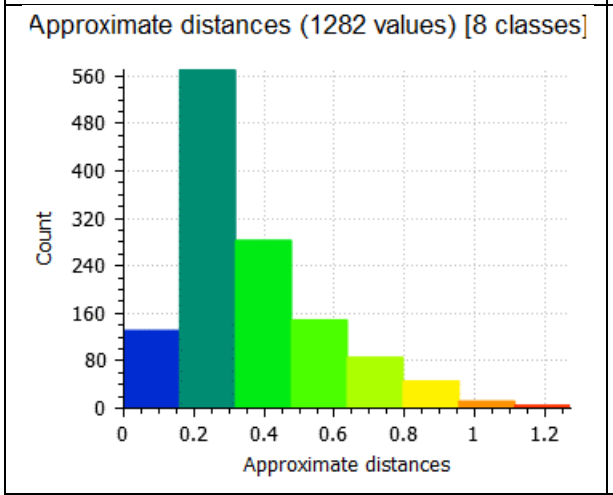

Tree4

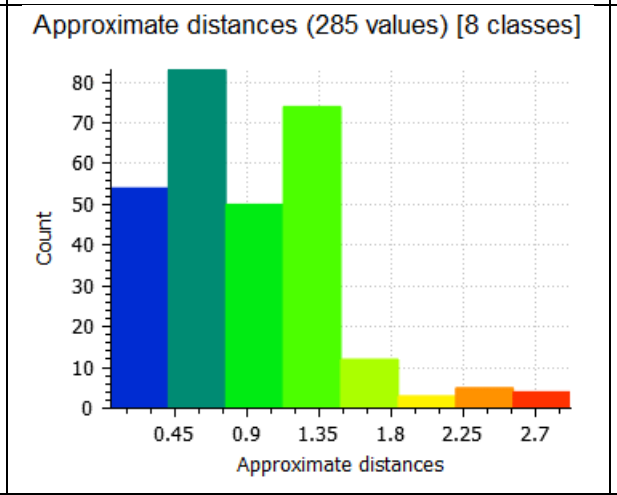

Tree5

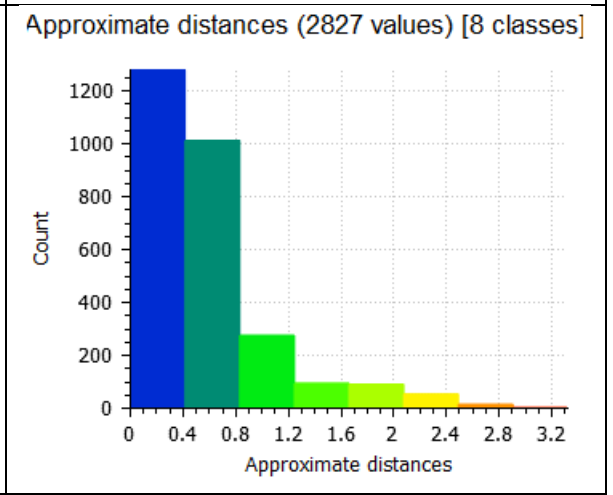

Tree6

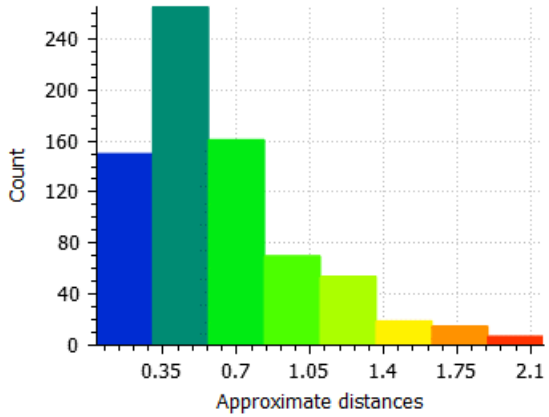

Tree7

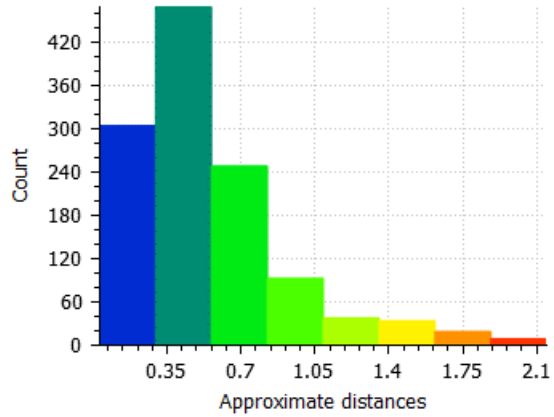

Tree8

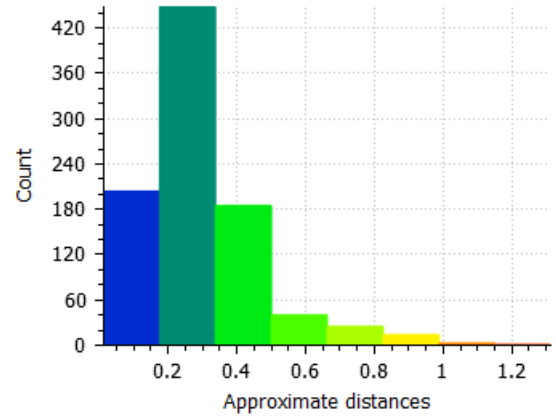

Tree9

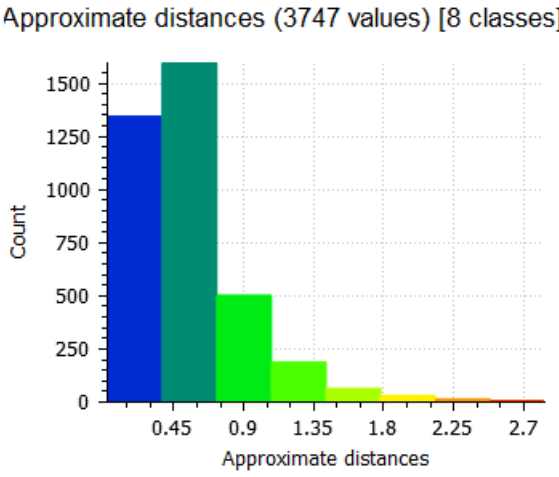

Tree10

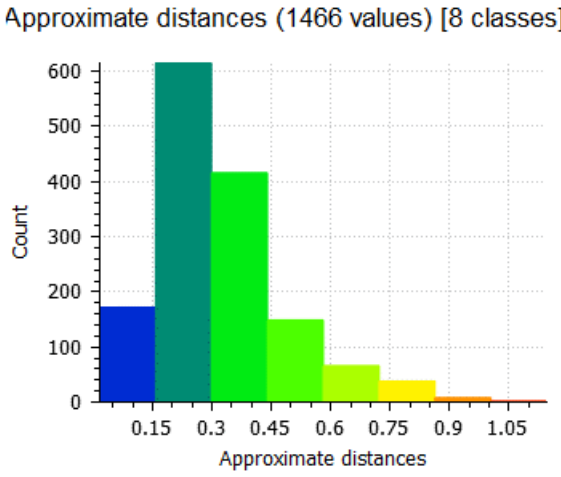

Tree11

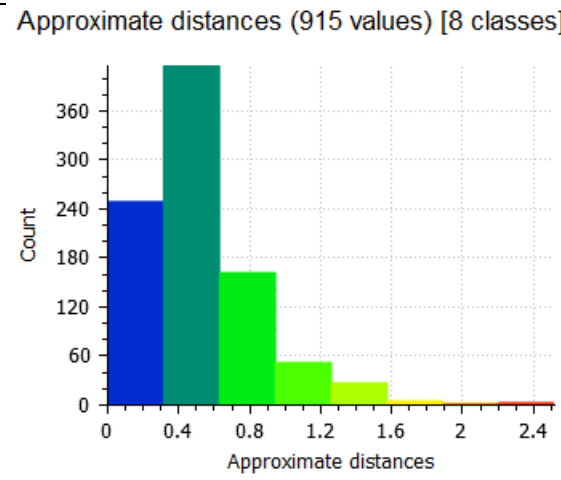

Tree12

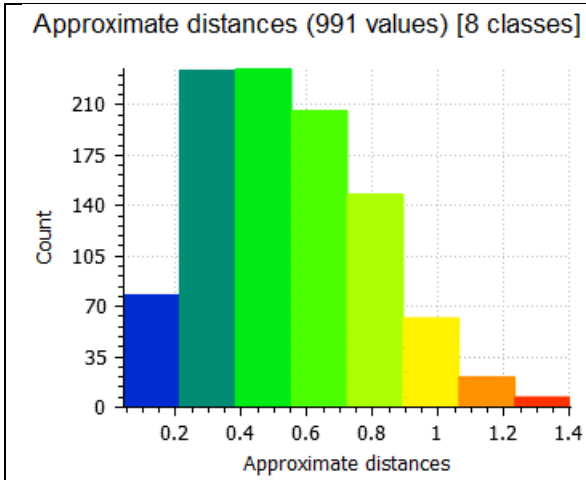

Tree13

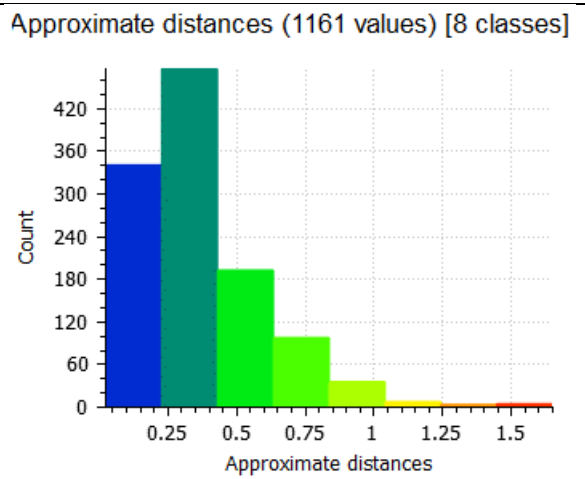

Tree14

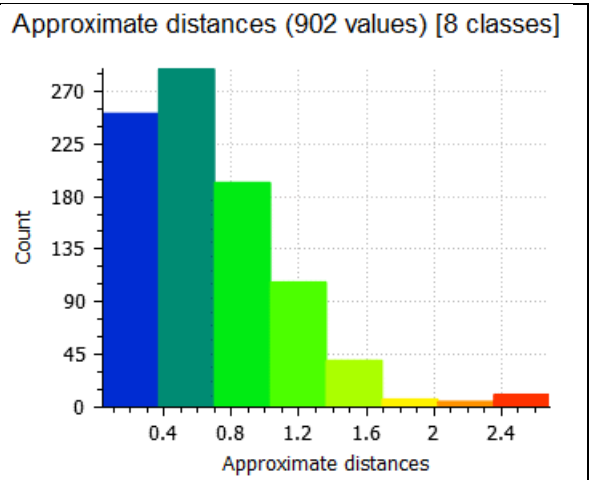

Tree15

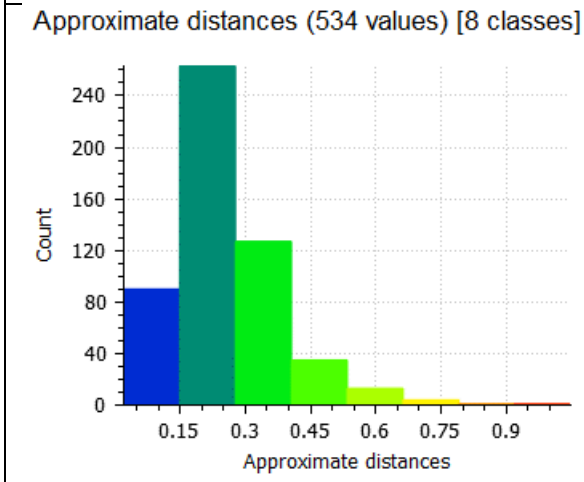

Tree16

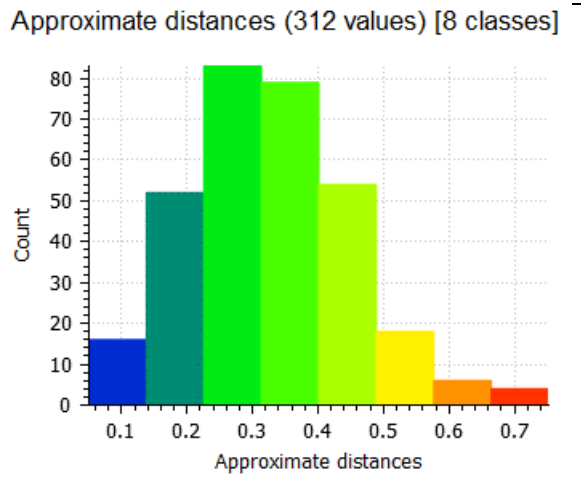

Tree17

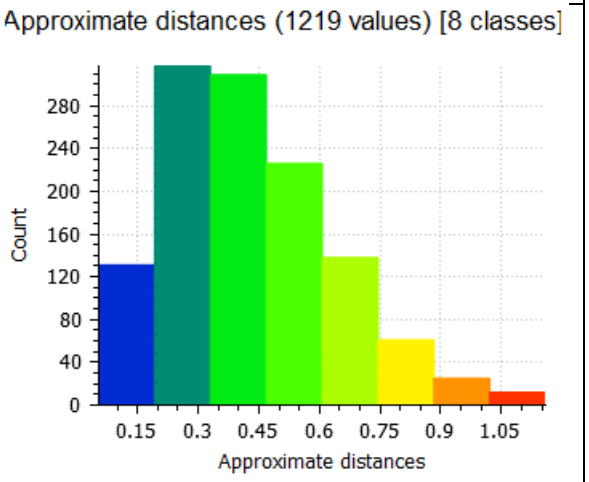

Tree18

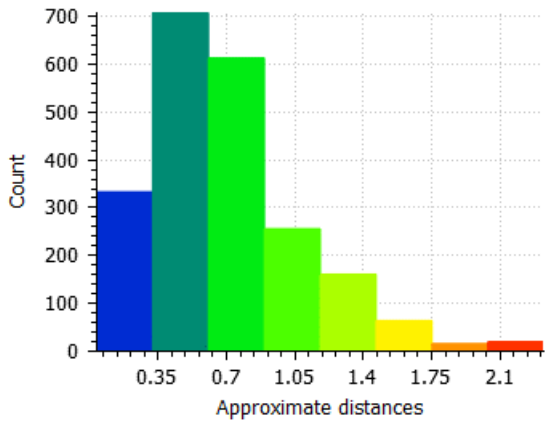

Tree19

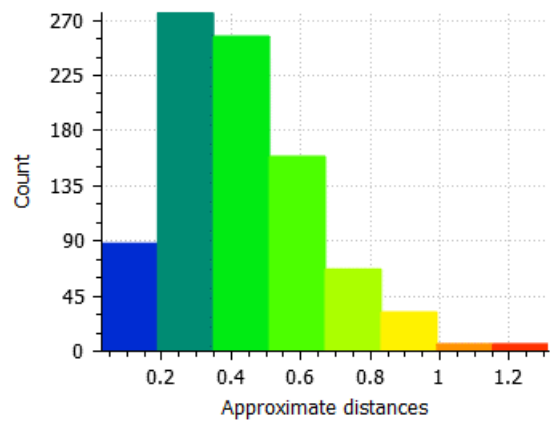

Tree20

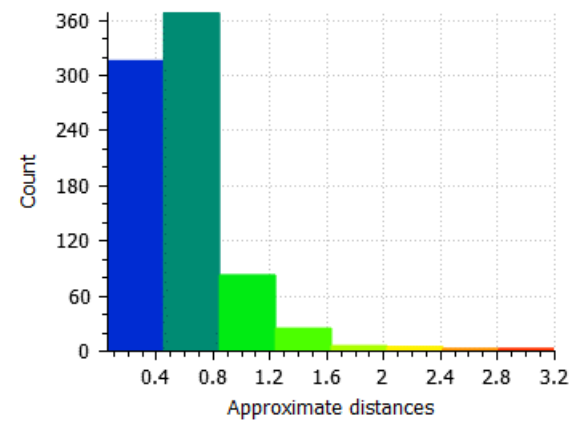

Tree21

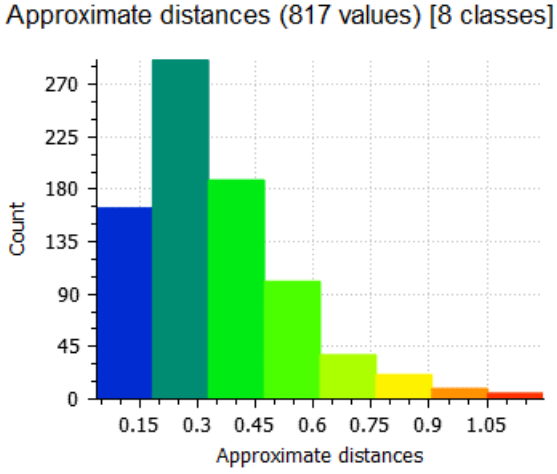

Tree22

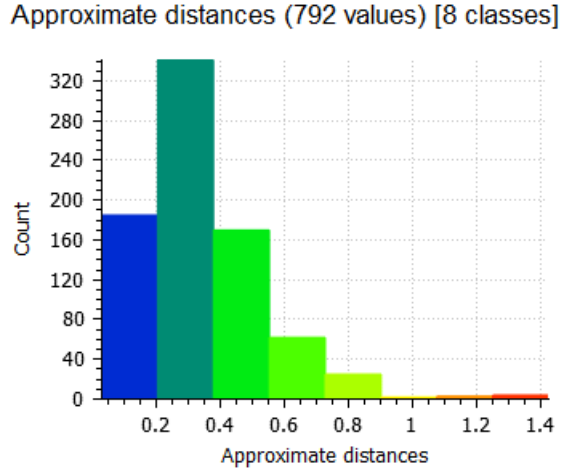

Tree23

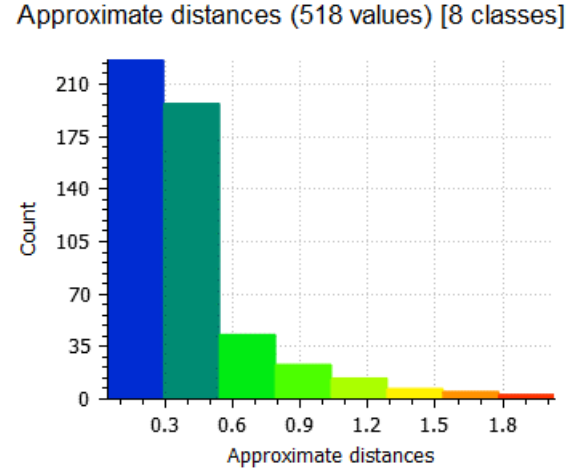

Tree24

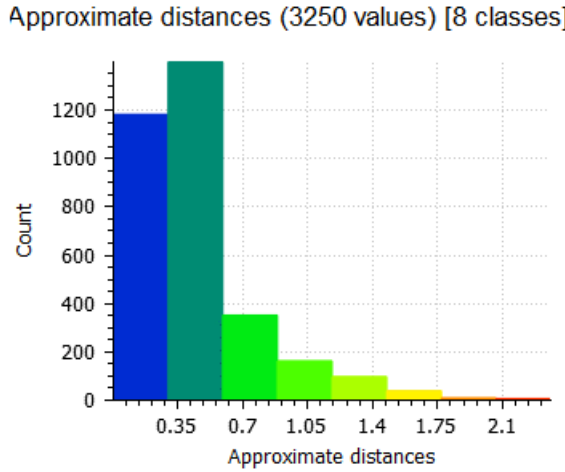

Tree25

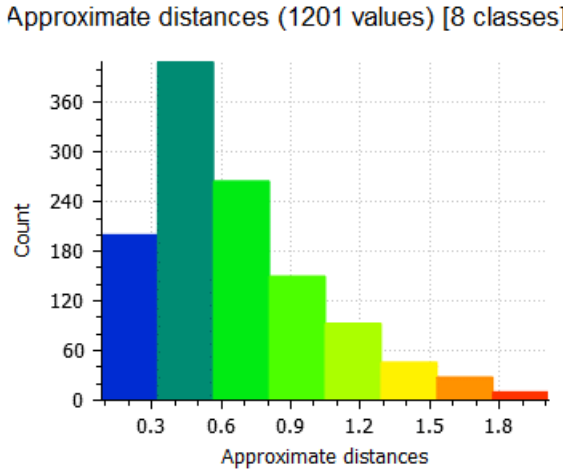

Tree26

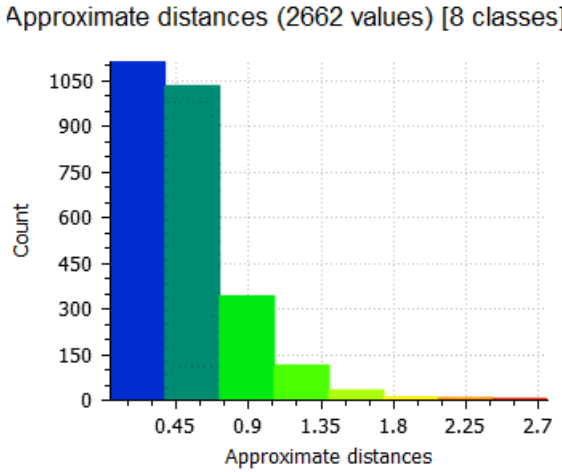

Tree27

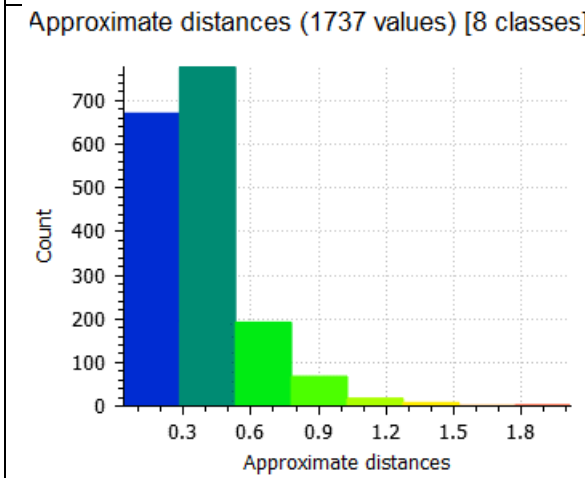

Tree28

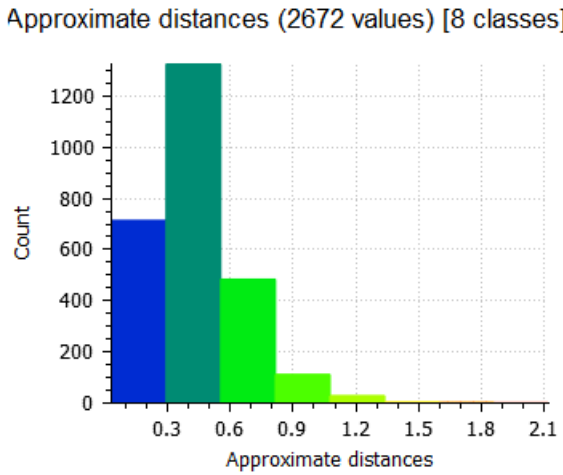

Tree29

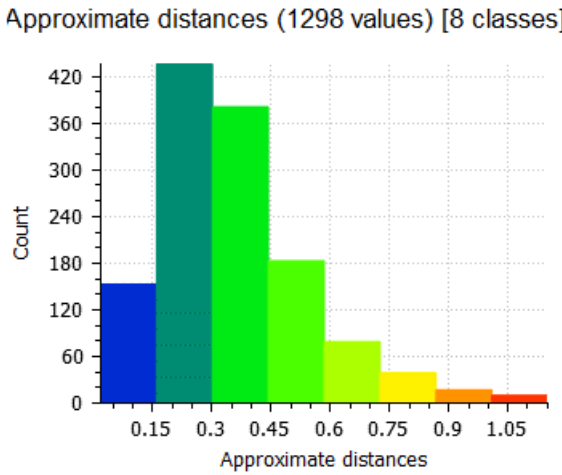

Tree30

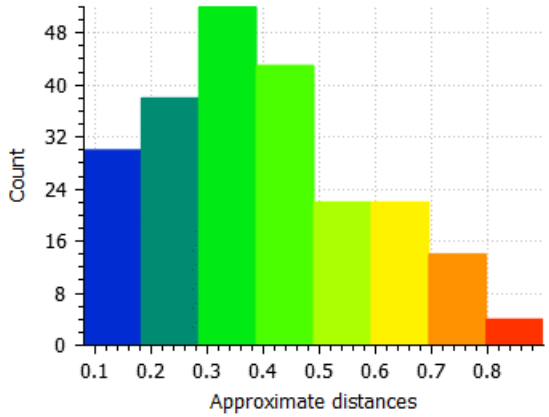

Tree31

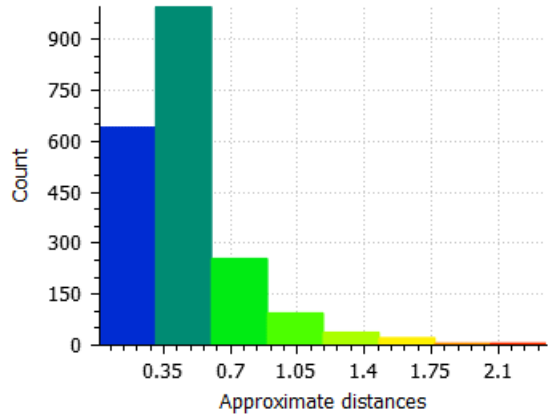

Tree32

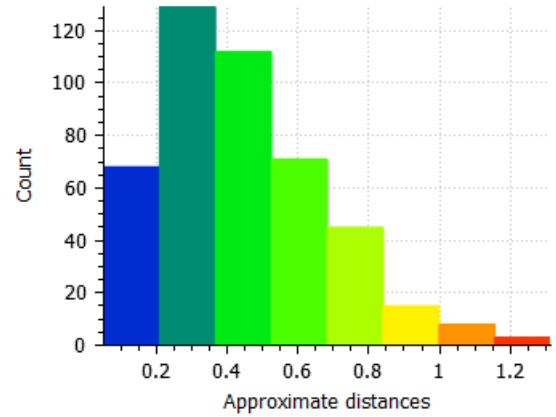

Tree33

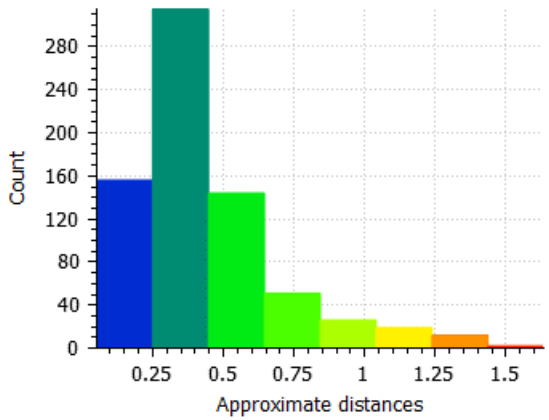

Tree34

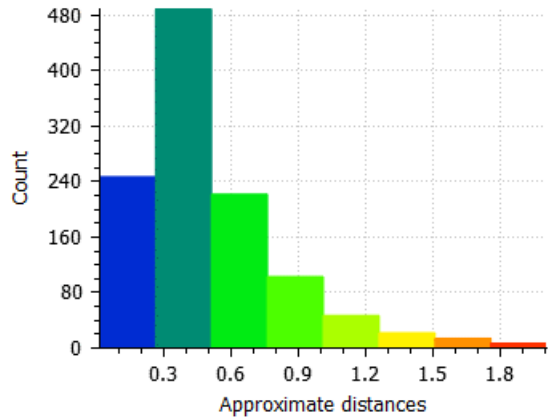

Tree35

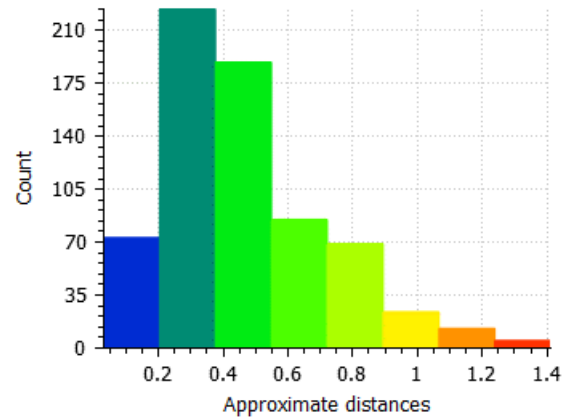

Tree36

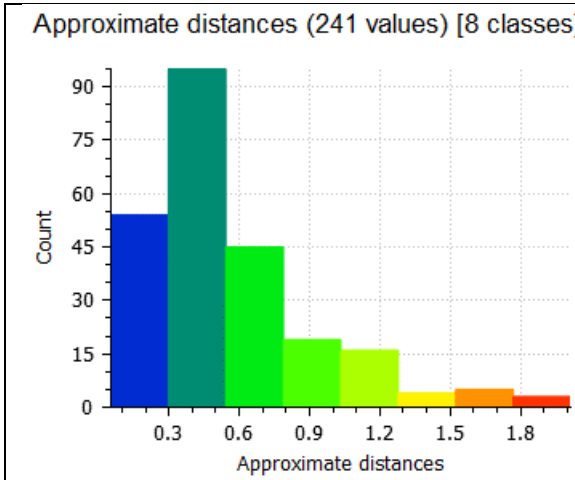

Tree37

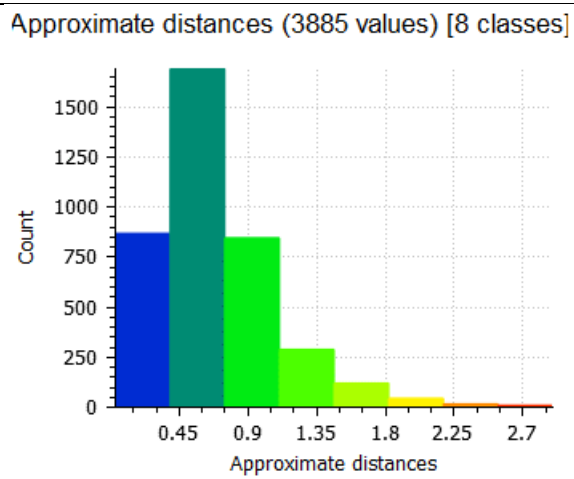

Tree38

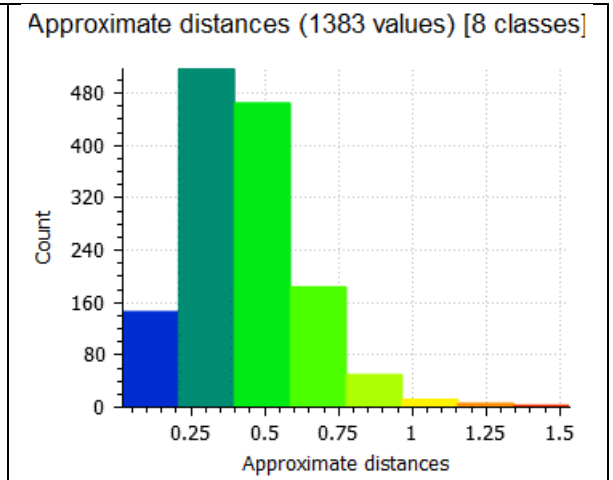

Tree39

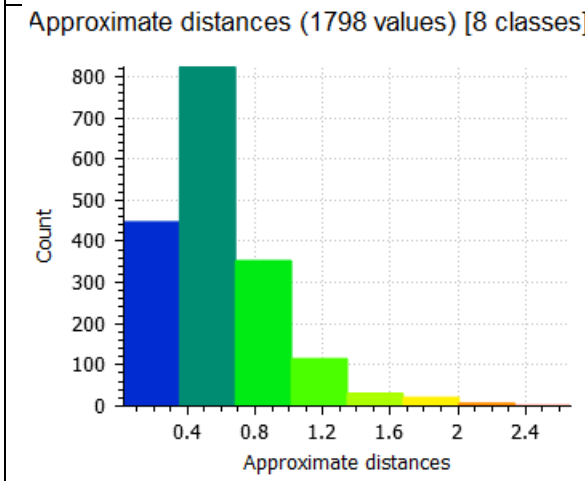

Tree40

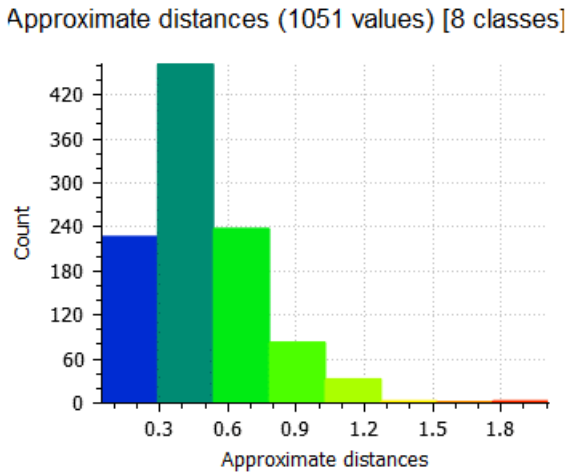

Tree41

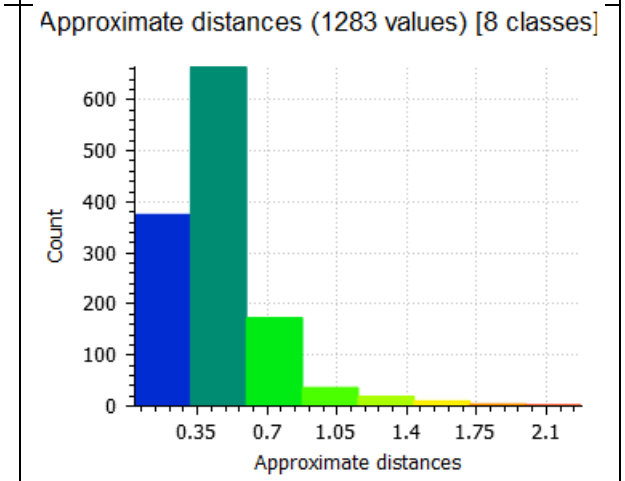

Tree42

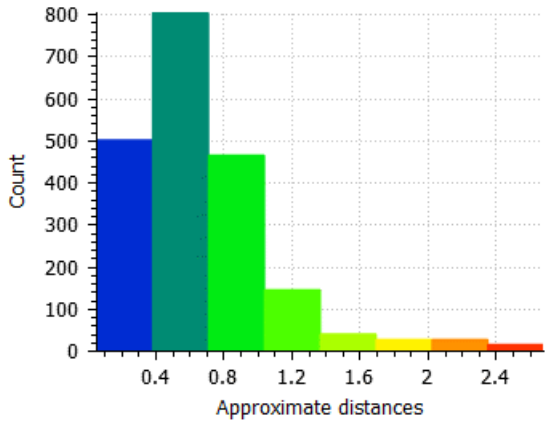

Tree43

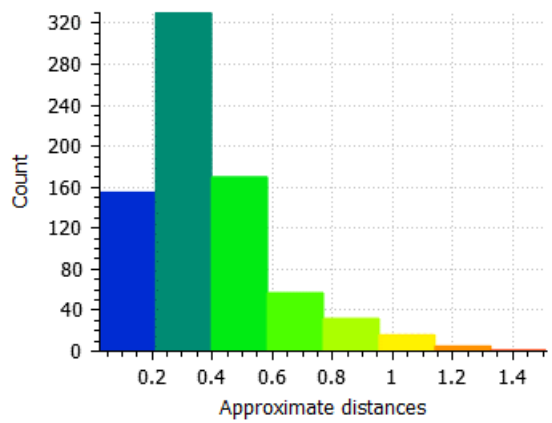

Tree44

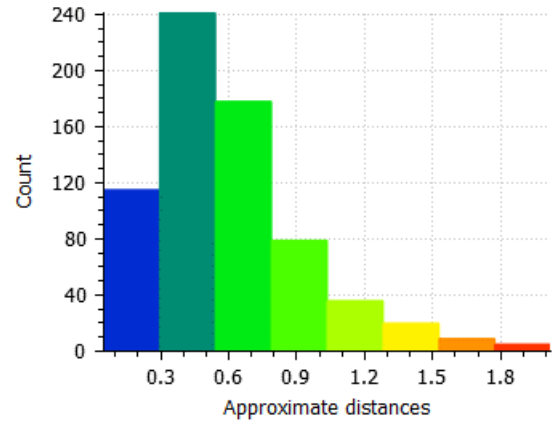

Tree45

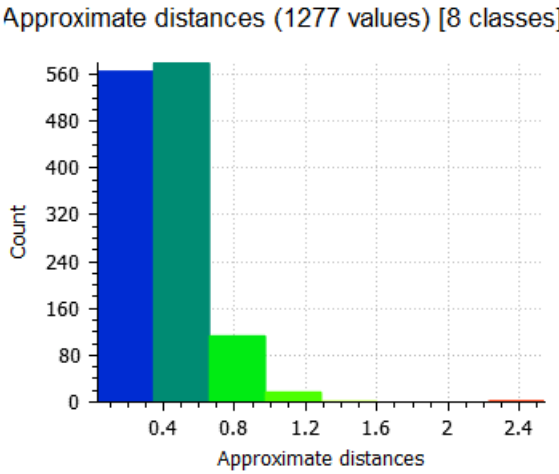

Tree46

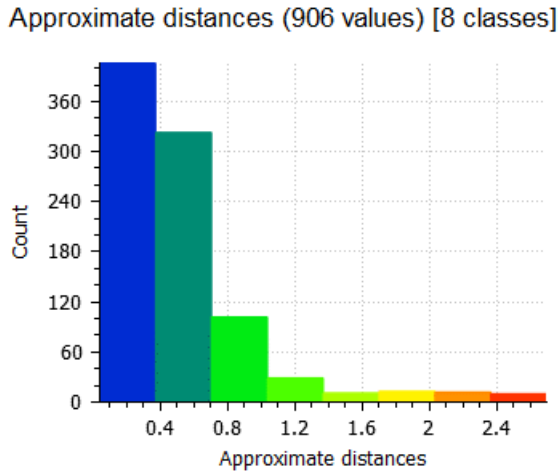

Tree47

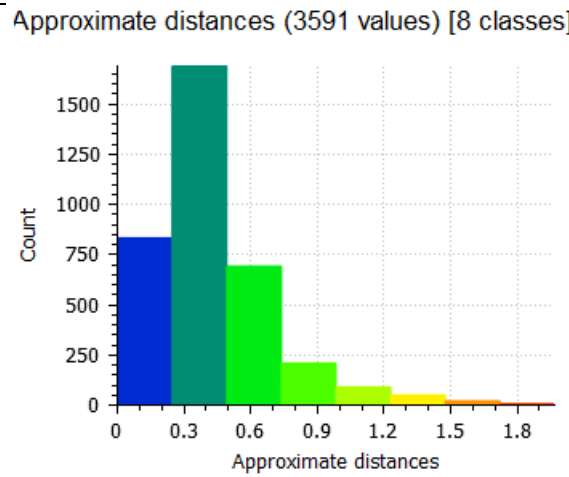

Tree48

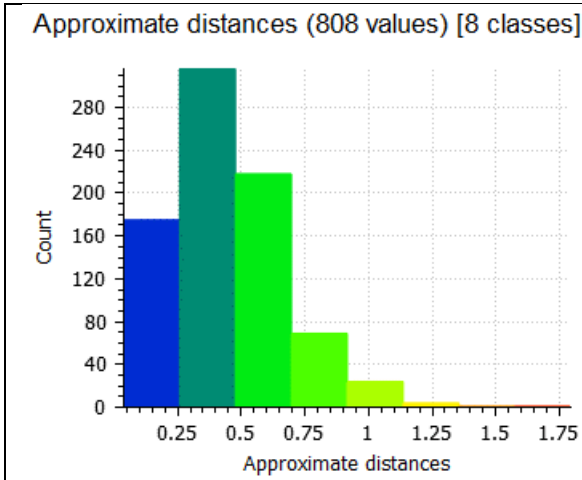

Tree49

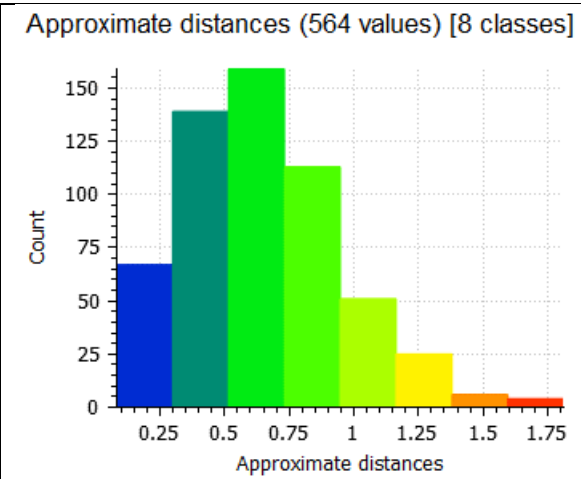

Tree50

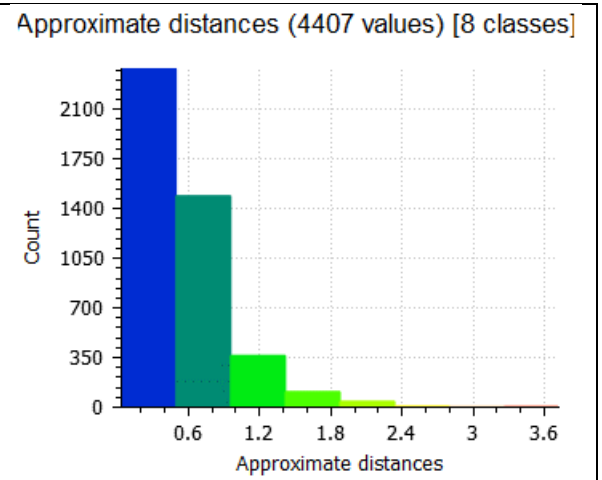

Tree51

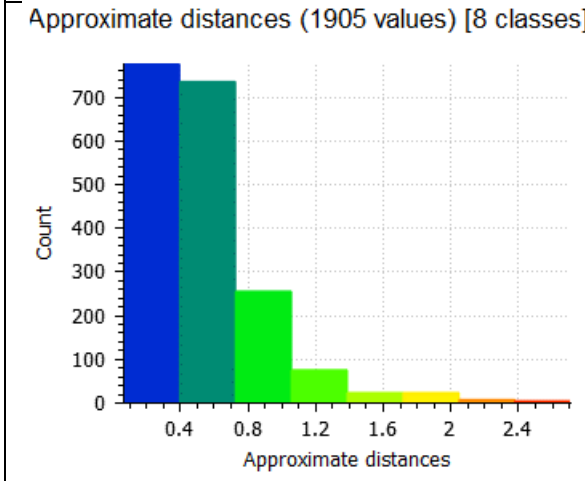

Tree52

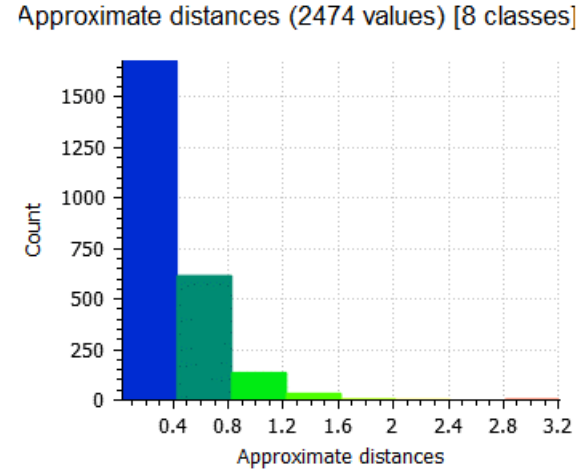

Tree53

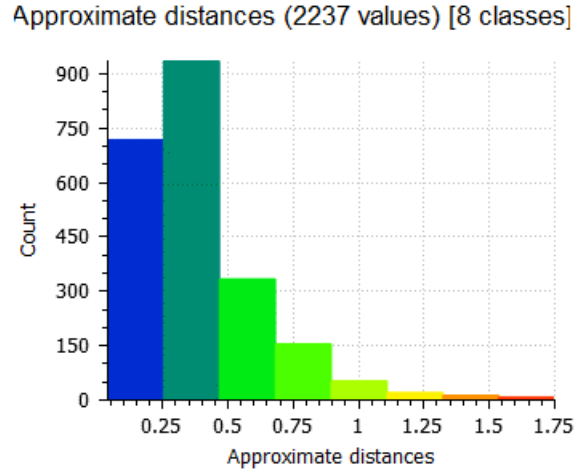

Tree54

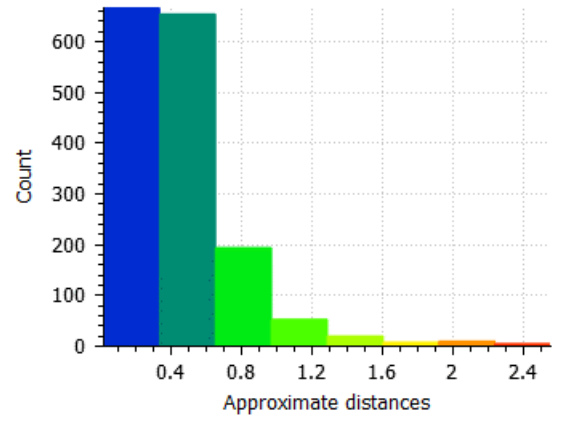	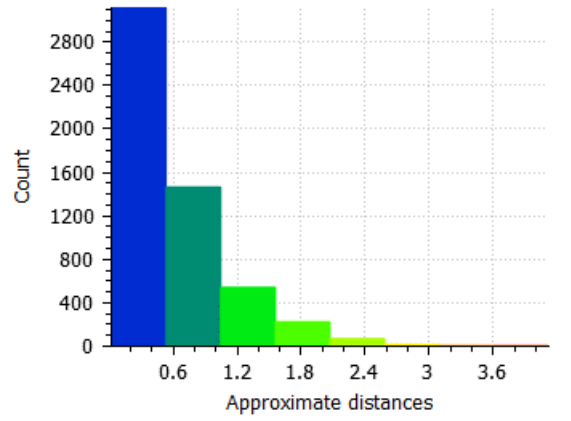	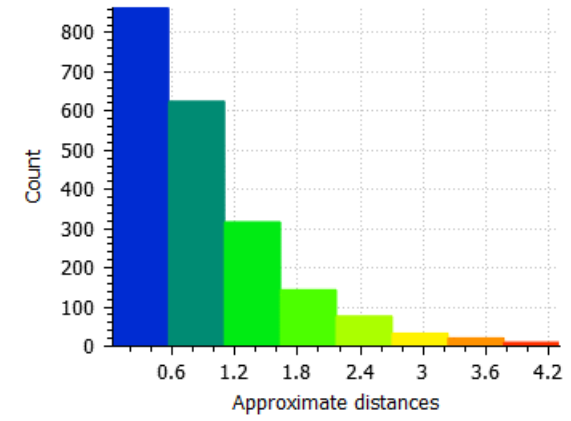
Tree55	Tree56	Tree57
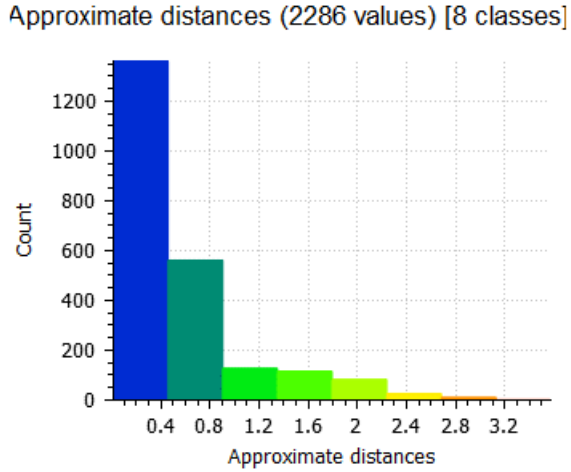	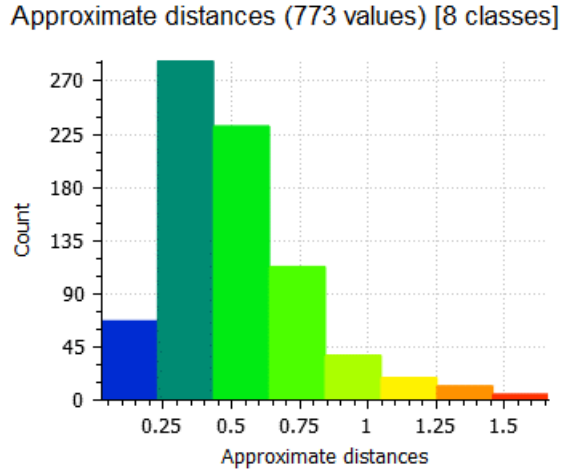	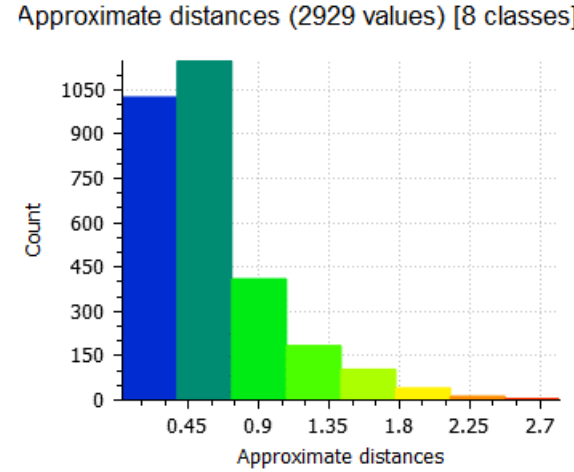
Tree58	Tree59	Tree60

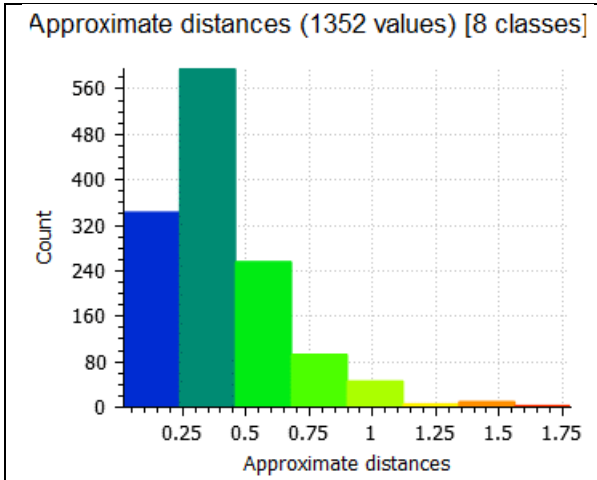

Tree61

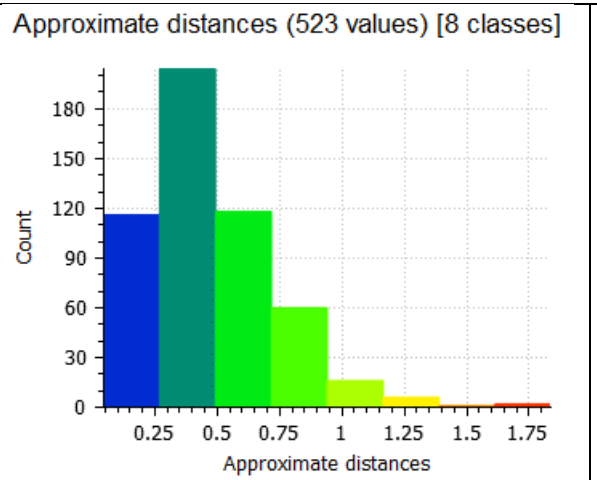

Tree62

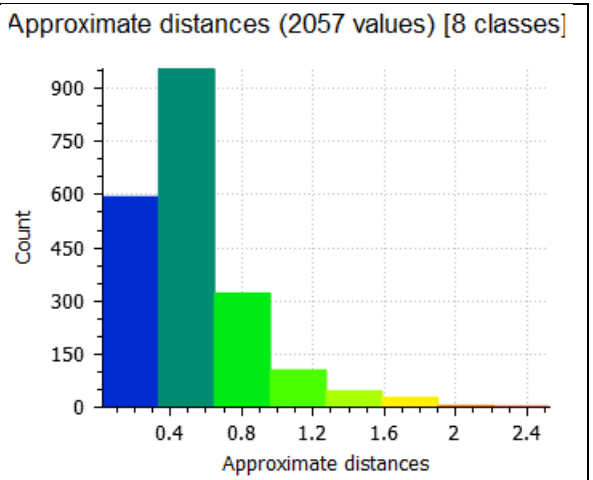

Tree63

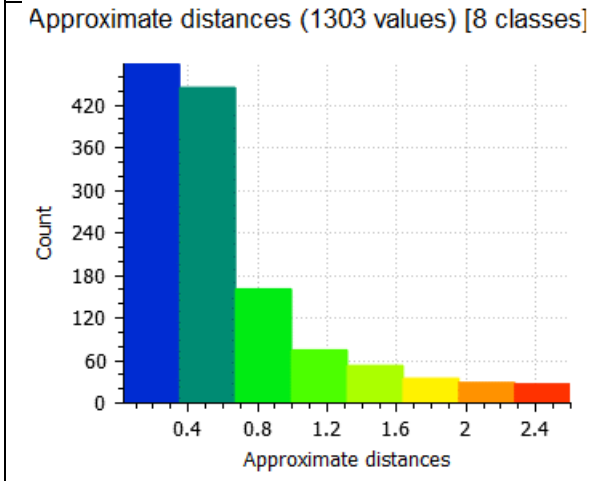

Tree64

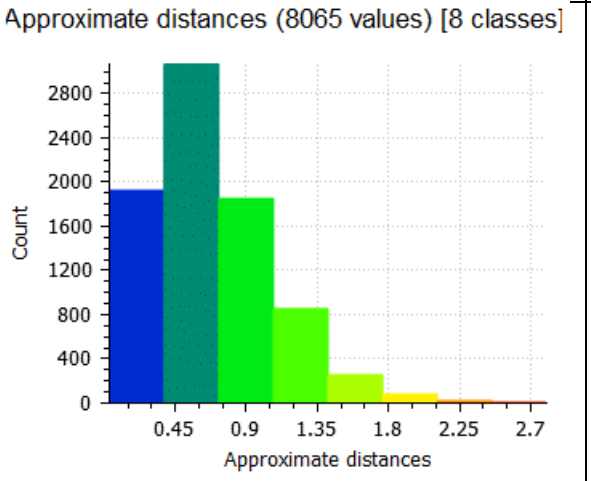

Tree65

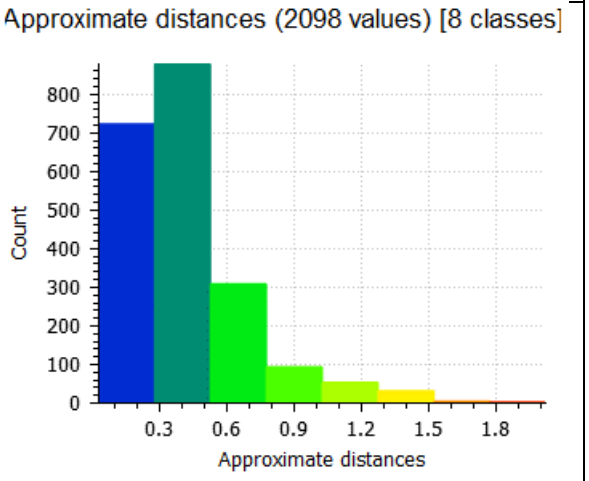

Tree66

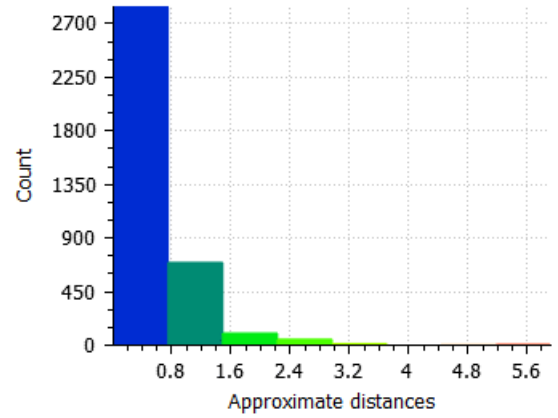

Tree67

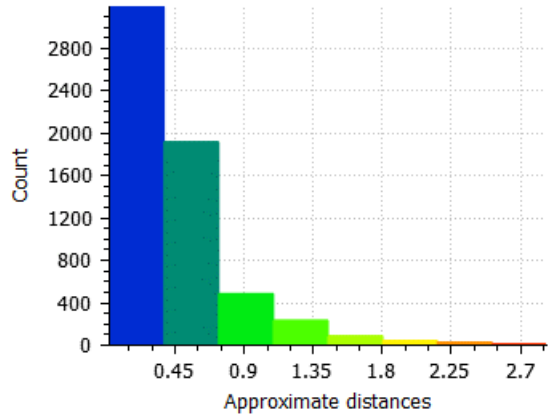

Tree68

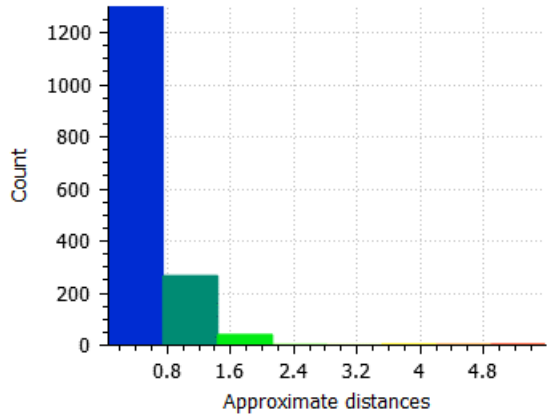

Tree69

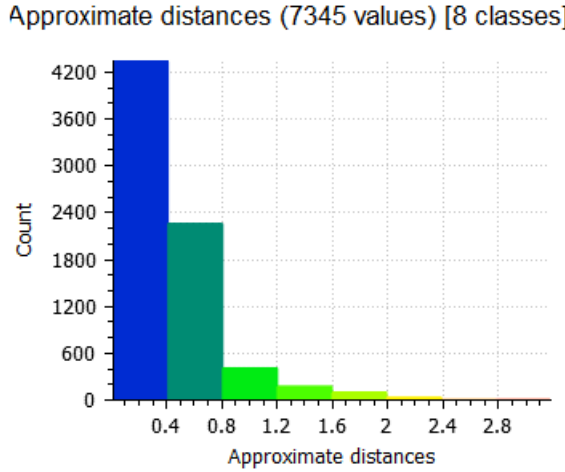

Tree70

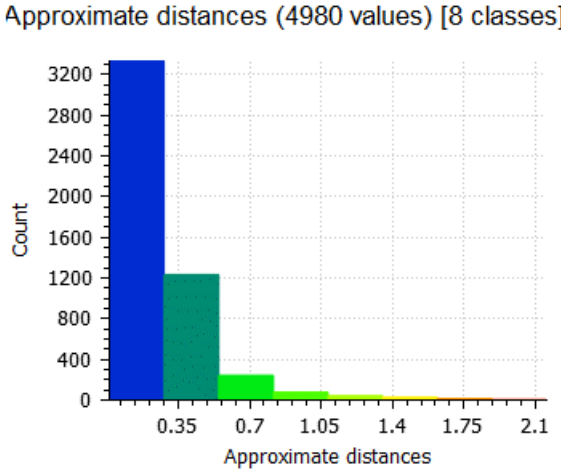

Tree71

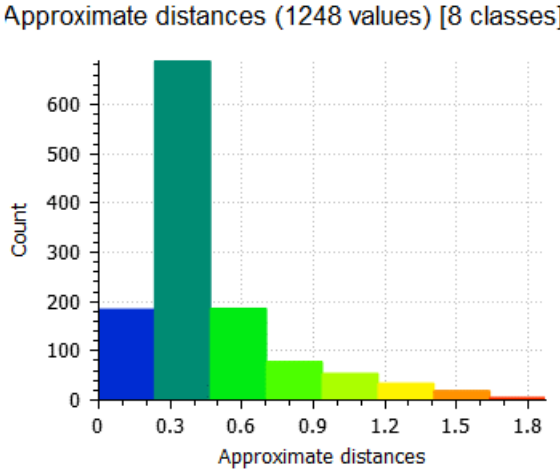

Tree72

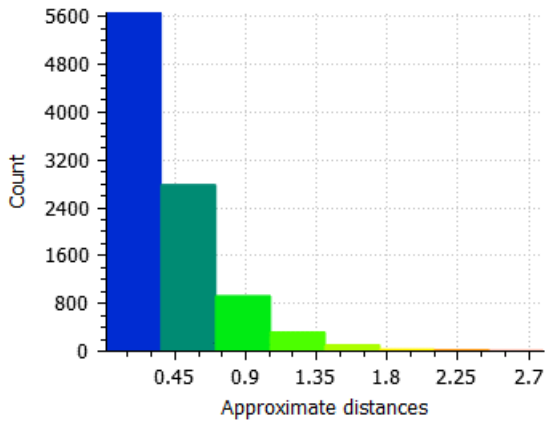

Tree73

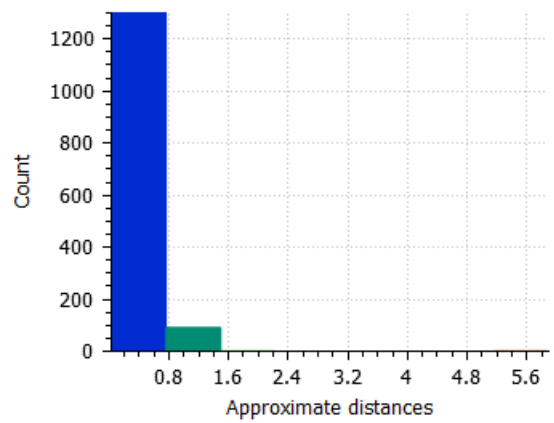

Tree74

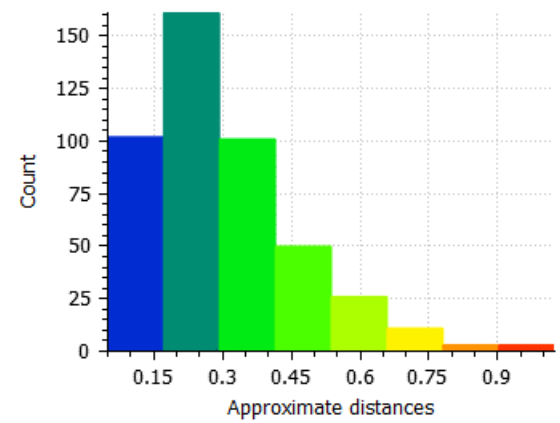

Tree75

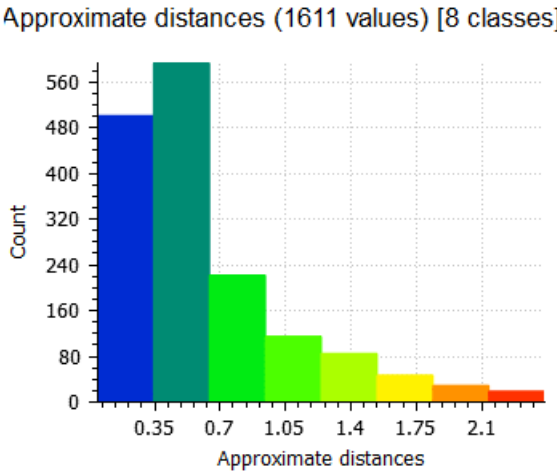

Tree76

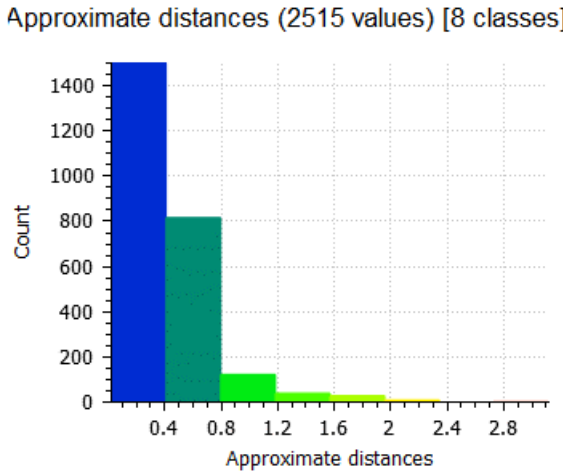

Tree77

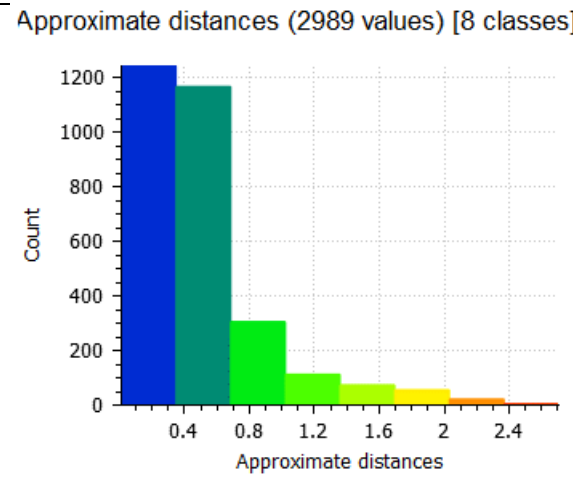

Tree78

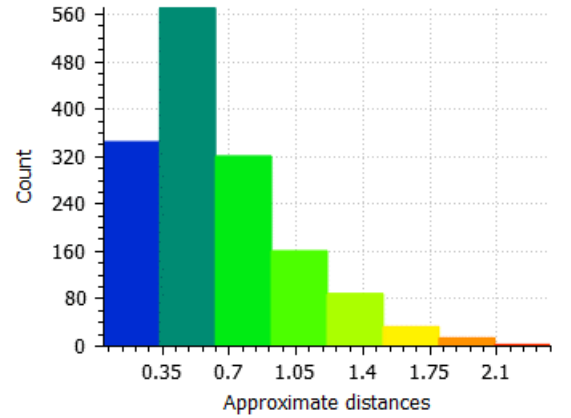	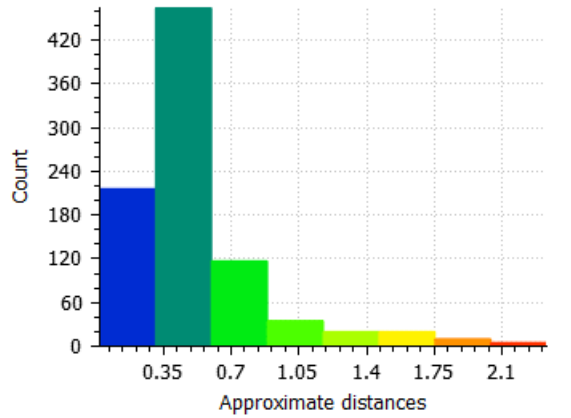	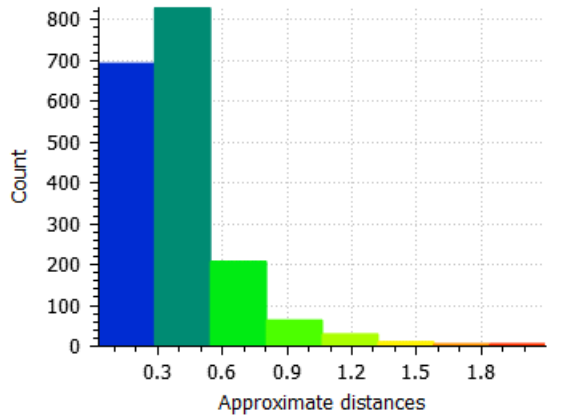
Tree79	Tree80	Tree81
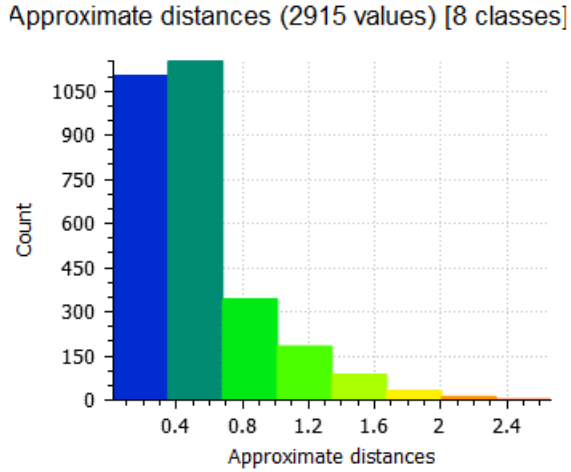	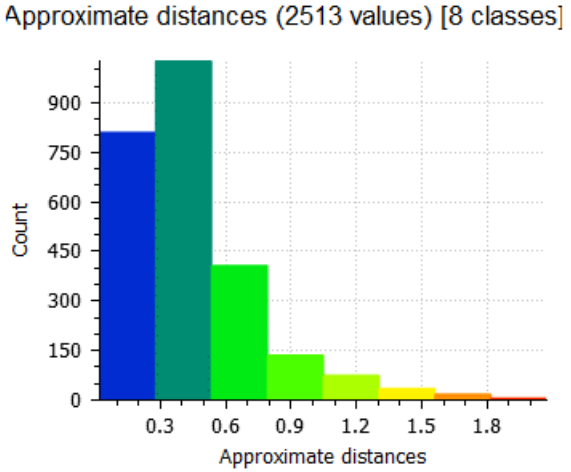	
Tree82	Tree83	